NON-LINEAR TIME VARYING MODELING FOR PHASE NOISE

NON-LINEAR TIME VARYING MODELING FOR PHASE NOISE IN OSCILLATORS BASED ON A DISCRETE RECURSIVE APPROACH

By

ANDREW LEUNG, B.Sc.

A Thesis

Submitted to the School of Graduate Studies

in Partial Fulfilment of the Requirements

for the Degree

Master of Applied Science

McMaster University

MASTER OF APPLIED SCIENCE (2005) McMaster University

(Electrical and Computer Engineering) Hamilton, Ontario

TITLE: Non-Linear Time Varying Modeling for Phase Noise in Oscillators Based On a Discrete Recursive Approach

AUTHOR: Andrew Leung, B.Sc. (University of Waterloo)

SUPERVISOR: Professor C. H. Chen

NUMBER OF PAGES: x, 107

ABSTRACT

A unique approach for the modeling of phase noise is examined in this thesis. In previous work regarding phase noise theory, the memory property of phase is virtually ignored. The thesis introduces the Discrete Recursive Procedure (DRP): a systematic approach or methodology to predict phase noise using a discrete recursive algorithm taking into account the memory property of phase. This discrete recursive algorithm is a general extension of the Linear Time Varying (LTV) model and is referred to as the Non-Linear Time Varying (NLTV) model.

Simulations are performed using the DRP method. Phase fluctuation comparisons are made between the LTV and the NLTV models for an ideal oscillator. The simulation results show that the NLTV model taking into account the memory property of phase makes more realistic phase noise predictions than the LTV model for asymmetrical Impulse Sensitivity Function (ISF) cases. Phase noise simulation results using the NLTV model are given for a modified 810-MHz CMOS cross-coupled LC oscillator design. At 90 kHz offset, the simulation prediction (-89 dBc/Hz) and the measurement readings (-93 dBc/Hz) are closely matched with a difference of approximately 4 dBc/Hz while the CAD simulation prediction (-101.8) has a difference of 9 dBc/Hz from the measurements. In the phase noise simulation for the 62-MHz BJT Colpitts oscillator design, the NLTV model predicts a -26 dBc/decade and –19.5 dBc/decade for the flicker noise and thermal noise regions in accordance with the theoretical –30 dBc/decade and –20 dBc/decade slopes.

ACKNOWLEDGEMENTS

I would like to thank Dr. C. H. Chen, my supervisor, for the help and guidance in my thesis research. His innovative and insightful ideas were essential to the completion of this thesis. I thank Dr. S. Naseh for his help in the phase noise measurements for the cross-coupled CMOS oscillator. I also would like to thank people in the Microelectronics Research Group for the support, assistance, suggestions, and ideas in my research work.

I wish to thank Dr. M. Bakr and Dr. S. Hranilovic for acting as my thesis defense committee members. I am also grateful to the Canadian Microelectronics Corporation (CMC) for arranging the fabrication of the test chips and the McMaster University Graduate Fellowship program for the financial support of this research.

Last, but not least, I would like to thank my parents for their encouragement and continuing support in my academic pursuits.

TABLE OF CONTENTS

LIST OF FIGURES

LIST OF TABLES

Chapter 1

INTRODUCTION

1.1 TECHNOLOGY AND INDUSTRY

Oscillators are an integral part of radio frequency (RF) and digital devices. The basic purpose of the oscillator is to generate an oscillating output. Most oscillators are developed using spiral inductors or crystals to attain stable oscillation. Practical applications of oscillators include the following: communication systems where periodic signals are used as information carriers, digital computer and control systems that are controlled by clock pulses, and test systems where periodic waveforms are used to characterize electronic devices. They can be found in many different types of electronic equipment. A quartz watch uses a quartz oscillator to keep track of the time. A radio transmitter uses an oscillator to create the carrier wave for the AM station and the AM radio receiver to tune into the station [1].

In the last few decades, there has been tremendous growth in the communications industry as new and inexpensive wireless services have emerged due to the advancements in digital signal processing, RF circuit fabrication, large scale circuit integration, and digital switching techniques. There also has been convergence of wireless and the Internet through broadband communications [2].

During the past few years the oscillator market has been on a decline. In 2002, the total worldwide crystal and oscillator revenue decreased to 2.3 billion dollars from 2.7

billion the previous year [3]. There have been signs of reversal last year despite the continuing price erosion and consolidation. Next-generation oscillators are being developed by suppliers that combine high frequency and low noise in smaller packages. Discera Inc. has developed a micro-oscillator allowing multiple oscillators operating at different frequencies to reside on a single die. This oscillator is aimed at wireless applications and replaces the quartz crystals to save space, cost, and power [3].

The current goal of the industry is to achieve high performance oscillators that are compact in size, cheap to produce, and consumes less power.

1.2 COMMUNICATION SYSTEM

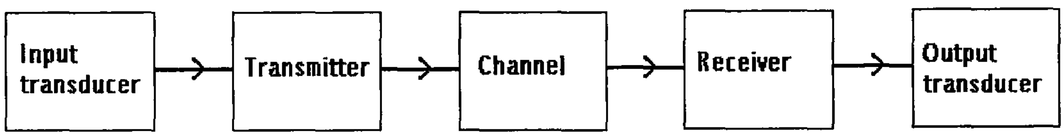

Fig. 1.1: Communication system.

Fig. 1.1 depicts a communication system consisting of the following components: the input transducer, transmitter, channel, receiver, and output transducer. The source sends a message in the form of a human voice, television picture, or any other data. The source information is converted by an input transducer into an electrical waveform known as the baseband signal. The transmitter modulates the baseband signal for more efficient transmission. The channel is a medium in which the output of the transmitter is sent. Distortion and noise is introduced in the channel. The receiver de-modulates and reprocesses the signal from the channel sent by the transmitter to be read by the output transducer. The task of the receiver is to extract the message from the distorted and noisy signal at the channel output through the use of filters. The output transducer receives the receiver output and converts the electrical signal to its original form.

1.3 MOTIVATION

Oscillators are fundamental components in the communication system (fig. 1.1). They are used inside the receiver and transmitter blocks in Radio Frequency (RF) applications to perform frequency conversions [4]. The goal in oscillator design is to develop high performance oscillators that have stable oscillation and minimal noise. The oscillator circuit should be compact in size, cheap to produce, and consume less power. Since oscillators are fundamental components in the communication system, it is vital to reduce the noise generated by the oscillator. **Phase noise** is the dominant noise component in oscillators and is the major obstacle in oscillator design. In order to understand phase noise, a system or model is created that describes the relationship between the input noise source and the noisy output (phase or voltage fluctuation). The source of phase noise in oscillators is the noise from the transistors and the parasitic resistance in the inductor-capacitor resonator. The noise sources (thermal and flicker noise) are the input for the phase noise system. The output of the system due to the injection of the input is the voltage or phase fluctuation leading to phase noise.

The first phase noise model described the relationship between the input noise current and the output voltage fluctuation as a linear time invariant (LTI) system and is known as the Leeson-Cutler model. In the early stages of phase noise research, many phase noise theories were built around the LTI system assumption [6]-[14].

A. Hajimiri and T. Lee introduced a general theory of phase noise for oscillators by treating the system as a linear time-varying (LTV) system [5]. Consider fig. 1.2 where a current impulse (input) is injected into parallel LC oscillator. When the impulse is injected when the oscillator waveform is at its peak, there is only amplitude fluctuation and the phase remains unchanged. But when the impulse is injected when the waveform is at the zero-crossing point, we have maximum phase fluctuation and the amplitude is the same. Thus, the system is time varying since the output phase depends on the injection time [5].

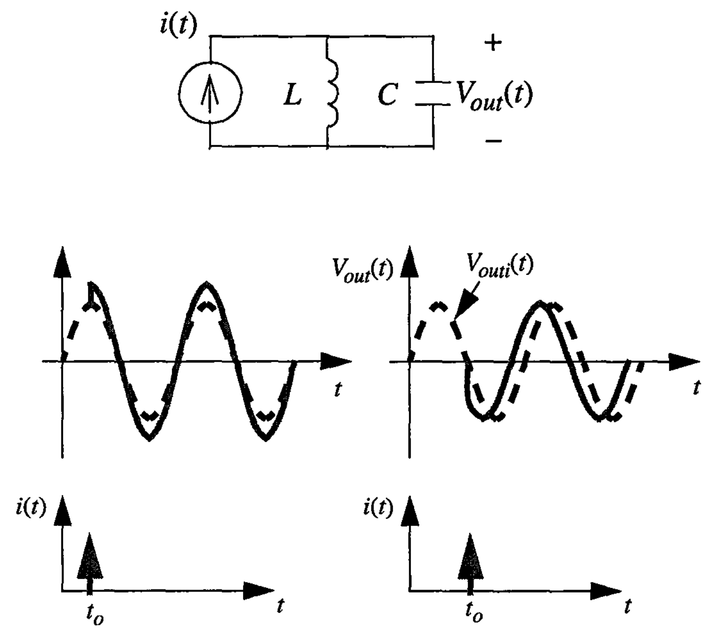

Fig. 1.2: Impulse injection and resulting phase shift.

Although this model correctly assumes the time varying nature, it neglects the memory property of phase. The memory property implies that the system remembers the phase changes caused by each noise injection. In other words, the phase is changed permanently after each and every noise injection. The model introduced in this work accommodates the time-varying nature but also takes into account the memory property present in the phase noise system. Unlike the two previous models, our model does not make an assumption for linearity.

Thus there are three important properties of the phase noise system:

1) Non-Linearity
2) Time variance
3) Memory

The LTI model neglects the time-varying nature of phase noise. The LTV model correctly accounts for the time-varying property but neglects the memory property. Our Non-Linear Time Varying (NLTV) model accommodates the memory and time-varying properties of phase and is more general since we treat the system as non-linear. The Discrete Recursive Procedure (DRP) is developed to implement the NLTV model algorithm and to provide a systematic guideline to calculate phase noise.

1.4 STRUCTURE OF THESIS

Chapter 2 provides background information on oscillators and three common design topologies: CMOS differential LC oscillator, Colpitts LC oscillator and the 5-Stage Ring oscillator. The CMOS differential LC and Colpitts LC oscillator topologies are used in Chapter 5 for phase noise simulation. The source of phase noise in oscillators is the noise from the transistors or devices. Two types of device noise: thermal and flicker are discussed extensively in Chapter 3. Chapter 4.1 and 4.2 are brief reviews of the Leeson-Cutler LTI theory and the LTV phase noise theory developed by A. Hajimiri and T. Lee. In Chapter 4.3 we introduce our phase noise theory taking into account the memory property of phase (the NLTV model). Chapter 4.4 introduces the Discrete Recursive Procedure (DRP): a systematic way to predict phase noise using the NLTV model to describe the phase noise system. The DRP simulation generates a phase noise output and uses the device noise (thermal and/or flicker noise) as input. The Fast Fourier Transform (FFT) tool used in Matlab for phase noise simulation is discussed in Chapter 4.5. Phase fluctuation DRP simulation results are given in Chapter 5.2. Phase fluctuation comparisons are made between the LTV and NLTV models to show how the memory property and phase fluctuation plays a role in realistic phase noise prediction. In Chapter 5.3, phase noise DRP simulation results using the NLTV model are given for a modified 810-MHz CMOS cross-coupled LC oscillator design. The simulation results for the NLTV model are compared against the corresponding measured results. Phase noise simulation for a BJT Colpitts LC oscillator is shown in Chapter 5.4 to show the phase noise characteristics due to $1/f$ and thermal noise for the NLTV model. In Chapter 5.5 a cross-coupled 1-MHz CMOS oscillator design example is used for the NLTV model to compare the phase noise results for different flicker noise models introduced in Chapter 3. This thesis concludes with the final chapter discussing the implications of the new NLTV model.

Chapter 2

OSCILLATOR BASICS

2.1 OSCILLATOR INTRODUCTION

There are several ways or methods to describe the operation of the oscillator. In other words, there are different points of views concerning how an oscillator functions. When designing an oscillator we can choose any one view (or method) to describe the oscillator since they are all equivalent. In this section we will look at two of the most popular methods to model oscillators. We can model the oscillator using any one of the following two popular methods:

1) 2-port view or feedback model with an amplifier and frequency selective filter element (tuned resonator circuit with coupling capacitors) in a positive feedback path. In order for this circuit to be an oscillator, the Barkhausen criterion must be satisfied. Fig. 2.1 shows the feedback model of the oscillator.
2) 1-port model or negative resistance model with an active non-linear network and a parallel resonator. For oscillation, the active network must generate negative resistance to match the parallel parasitic resistance of the resonator circuit [15]. Fig. 2.2 shows an *RLC* oscillator with an energy restorer that generates negative resistance that cancels out with the lossy resistance *R* of the *LC* resonator.

It should be emphasized that to model an oscillator, the feedback model or the negative resistance model can be used since they are essentially both equivalent.

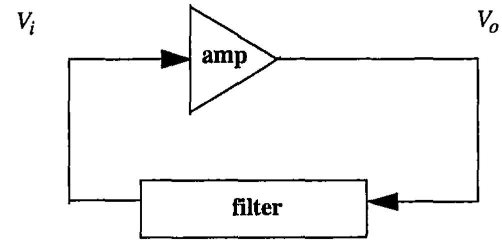

Fig. 2.1: Feedback oscillator model.

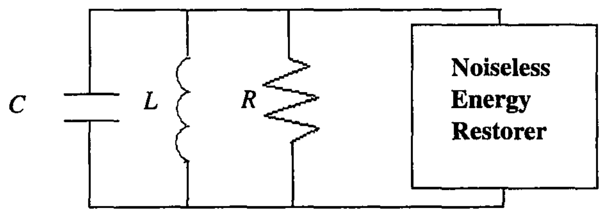

Fig. 2.2: Negative resistance oscillator model.

The feedback model is examined first. At the most general level, the oscillator can be modelled as a simple feedback system with an amplifier and a filter (fig. 2.1). The feedback filter signal is summed positively with the input signal giving us a positive-feedback loop. The gain of the feedback system is given by the following equation:

$$A_f(s) = \frac{A(s)}{1 - A(s)\beta(s)} \tag{2.1}$$

where A and β are the gain of the amplifier and filter respectively.

In order for this system to oscillate, the denominator of (2.1) must be zero. To understand this intuitively, assume that the denominator and input voltage V_i are zero (no external excitation). We then have $A(s)\beta(s) = 1$ and $V_o = A \cdot \beta \cdot V_o = V_o$, meaning that we have a sustained output when there is no input signal. The Barkhausen criterion for oscillation can be illustrated by

$$L(j\omega_o) = A(j\omega_o)\beta(j\omega_o) = 1\,. \tag{2.2}$$

In other words, the phase of the loop gain has to be zero and the magnitude of the loop gain should be unity at the resonant frequency ω_o [15].

Applying the Barkhausen criterion to oscillator circuits, we have two basic criteria for oscillation: the first is the loop gain must exceed unity at resonant frequency and the second is the phase shift around the loop (through the amplifier and filter circuits) must be an integer multiple of 360 degrees.

From fig. 2.1, the filter block consists of the tuned LC resonator circuit and the coupling capacitor network. The resonator is used to set the frequency at which the oscillator operates (resonant frequency). Tuned resonator circuits are usually implemented using an inductor with coupling capacitors for satisfying the phase shift criteria.

The amplifier gain and relevant circuit components must be designed, so that the loop gain exceeds unity at resonant frequency. The reason that the loop gain must exceed unity is because of the start-up operation of the oscillator. When the power is first applied to the oscillator, there is a sudden voltage change that excites the resonator and the signal starts to buildup due to the excess gain (greater than unity loop gain). The non-linear amplifier limits the loop gain to unity and at this point we have reached steady-state operation. The tuned resonator *LC* circuit then causes the entire oscillator system to oscillate at its resonant or natural frequency. This automatically satisfies the Barkhausen phase shift criteria because operating at the resonant frequency implies that the reactance (imaginary impedance) of the *LC* circuit cancels out thereby leaving zero phase shift [15].

The negative resistance model of the oscillator is examined next. An ideal tuned circuit has no lossy elements and would oscillate forever because there is no loss of energy. In reality, there are lossy elements in the circuit that would cause the oscillation to decay over time (e.g. damped sinusoidal signal). An ideal parallel tuned *LC* oscillator would oscillate endlessly with a frequency of $\frac{1}{\sqrt{LC}}$. However, a practical *LC* oscillator contains resistance that dissipates the waveform, so the *LC* oscillator can be modeled as a parallel *RLC* circuit where *R* is the equivalent resistance seen by the parallel LC network. In order for the *RLC* circuit to oscillate without damping, we need an active element to restore the energy that was loss by the resistance. In other words, this active network must provide negative resistance that cancels out the lossy resistance (fig. 2.2).

The active element in the oscillator circuit is the amplifier we discussed earlier. The amplifier maintains oscillations by supplying energy to offset the energy lost. This condition is equivalent to the Barkhausen loop gain criteria discussed earlier. Oscillators are essentially signal generators that produce periodic stable waveforms. This work primarily focuses on LC resonator oscillators that produce sinusoidal waves.

The design factors used for comparison between the different types of oscillators in this work include the frequency of operation, quality factor Q, and phase noise. For a parallel LC circuit, the frequency is defined by the values of inductor L and capacitor C. Trimmer (variable) capacitors can be used to vary the capacitors to tune the circuit for various frequencies.

The quality factor Q is defined as the energy stored over the energy lost. It is given by $Q = \frac{X}{R}$ where X is the reactance of the inductor and R is the series lossy resistance of the inductor. It is found in experiments that a high Q implies more stable oscillation, lower phase noise and a well-defined bandwidth. Thus it is desirable to have the highest Q possible for the tuned resonator. Phase noise is the dominant noise component in oscillators and should be minimized as much as possible. The source of phase noise originates from the noise in the active devices and the parasitic components in the resonator. In the general case, high Q implies good phase noise performance.

T. Lee and A. Hajimiri developed a linear time varying (LTV) model for phase noise where the input is the noise from the device and the phase fluctuation in the time domain is the output [5]. This model is time varying: the phase fluctuation is dependent on when the intput noise is injected into the system. The LTV model predicts we can achieve minimum phase noise when the active network (or amplifier) remains off almost all the time and wakes up periodically to deliver current at the peaks of the oscillator voltage waveform for each cycle [16]. Research has been done on a method called "phase noise tuning" where phase noise performance can be traded for power dissipation [17].

2.2 CMOS DIFFERENTIAL LC OSCILLATOR WITH SPIRAL INDUCTORS

Fig. 2.3 shows the schematic for the cross-coupled CMOS differential *LC* oscillator. It is assumed that the differential stage current switches from one side of the circuit (M_3) to the other (M_2). The I_{tail} current in the schematic depicts this behavior. The tuned resonant *LC* circuit is also known as the tank because it stores energy in the oscillator. The I_{tail} current flows through the tank and as the tank voltage goes up to a certain point, the direction of the current flow through the tank will reverse completely (*LC* oscillator). The current in the tank is a periodic signal that changes with the tank voltage.

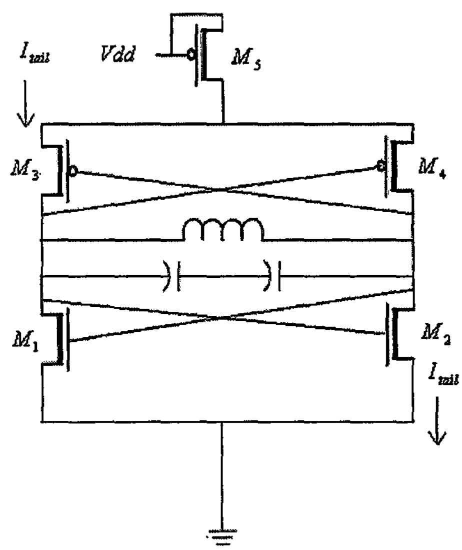

Fig. 2.3: CMOS differential oscillator.

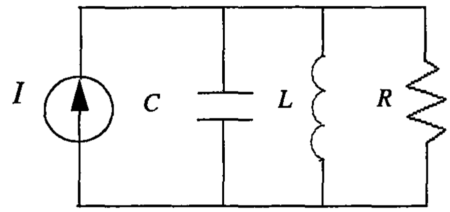

Fig. 2.4: Differential equivalent circuit.

The CMOS differential circuit can be modeled as a *RLC* tank with a current source switching between I_{tail} and its negation (fig. 2.4), where R_{eq} is the equivalent parallel resistance of the tank. Looking at it through the negative resistance model, the cross-coupled transistor pairs provide negative resistance that cancels the lossy resistance of the tank to provide oscillation. At the resonant frequency (determined by *L* and *C*) the reactances of the tank cancel out leaving the lossy resistance. Therefore the voltage across the tank can be approximated by

$$V \approx I_{tail} R_{eq} . \qquad (2.3)$$

Hence, the voltage across the tank *V* is a periodic signal generated by the differential oscillator. We are free to choose *L* and *C* to meet our desired frequency [18].

If on-chip spiral inductors (2 nH inductance) are used for the resonator, we can achieve a quality factor *Q* as high as 20 and achieve frequency around 2 GHz. *Q* is relatively high because spiral inductors reduce the lossy series resistance of standard inductor thereby increasing the percentage of energy stored to the energy dissipated [19]. However at higher frequencies (over tens of GHz), the *Q* becomes degraded. For such high frequencies, a microstrip line inductor should be used. The capacitor C can be tuned for frequency selection by using trimmer capacitor or varactor diodes where the capacitance is controlled by an applied voltage.

In general, symmetry in the circuit topology and in the oscillator voltage waveform help to reduce phase noise. Due to the differential and symmetrical nature of the CMOS cross-coupled oscillator, good phase noise performance can be achieved because noise in the two symmetrical half-circuits are partly correlated [18]. The use of the cross-coupled CMOS as opposed to a cross-coupled NMOS topology improves phase noise performance because of the improved rise and fall time symmetry in the oscillator waveform [18].

In essence, the property of symmetry is a good counter-measure against phase noise. A phase noise of –121 dBc/Hz at an offset of 600kHz from the carrier can be achieved in a 1.8 GHz system with on-chip spiral inductors [16].

2.3 COLPITTS & CLAPP LC OSCILLATOR

The bipolar Colpitts oscillator is shown in fig. 2.5. The oscillator can be thought as a feedback system with the tuned resonator. The resonator consists of an inductor and a capacitive voltage divider that couples energy from the emitter to the base. The feedback is provided by the tapped capacitor voltage dividers C_1 and C_2 [15].

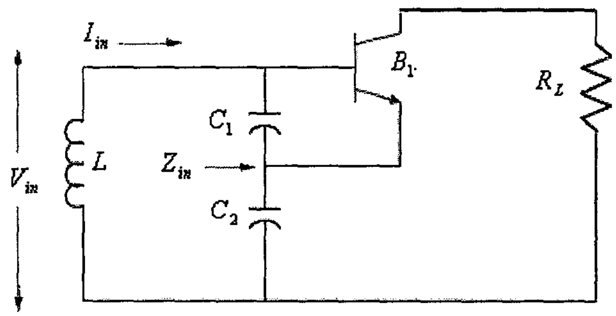

Fig. 2.5: Colpitts LC oscillator.

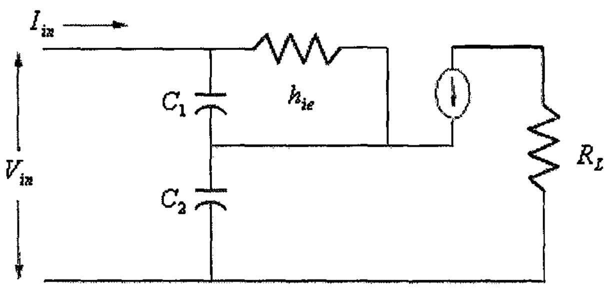

Fig. 2.6: Small signal colpitts model.

The negative resistance model is used to describe the operation of this oscillator. Fig. 2.6 shows the small signal equivalent circuit for the Colpitts oscillator. The input voltage V_{in} is the voltage across the inductor. This inductor is not ideal and would have a lossy resistance in series with it. In order for oscillation to occur in the negative resistance model, the amplifier network must provide negative resistance to cancel the effect of lossy components. Looking into the input voltage port, the input impedance is given by the following equation where the reactance $X_{C1} << h_{ie}$ is assumed [20],[21]:

$$Z_{in} = V_{in}/I_{in} \approx \frac{-g_m}{\omega^2 C_1 C_2} + \frac{1}{j\omega[(C_1 C_2)/(C_1 + C_2)]} \tag{2.4}$$

The input impedance consists of a negative resistance in series with a series capacitance. This negative resistance must cancel out the effect of the inductor series resistance R_s so we can set $R_s = \frac{g_m}{\omega^2 C_1 C_2}$. In order to have oscillation, the following equation must hold:

$$R_s \leq \frac{g_m}{\omega^2 C_1 C_2}. \tag{2.5}$$

Equation (2.5) affects the design because it limits the maximum values of the two capacitors. Setting $C_m = C_1 = C_2$ where C_m represents the value of the capacitors for maximum series capacitance and G is the maximum value of g_m, (2.5) can be re-written as:

$$\frac{1}{\omega C_m} > \sqrt{\frac{R_s}{G}}. \tag{2.6}$$

For oscillation in the Colpitts oscillator, the minimum reactance must be greater than the root of the ratio between the resistance of the inductor and the maximum transistor mutual conductance [20]. The feedback circuit (inductor and the two series capacitors) gives the following oscillation frequency

$$\omega_o = \frac{1}{\sqrt{L((C_1 C_2)/(C_1 + C_2))}} \quad . \tag{2.7}$$

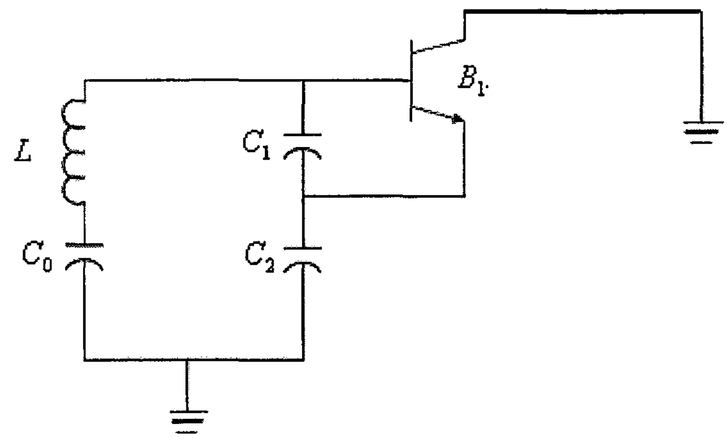

Fig. 2.7: Clapp oscillator.

The Clapp oscillator is a slight modification of the Colpitts oscillator with an extra capacitor C_0 in series with the inductor (fig. 2.7). Capacitors C_1 and C_2 can be chosen to satisfy the oscillation requirements (2.5), while the capacitor C_0 can be used to give us more design freedom by allowing us to adjust the oscillation frequency. The frequency of oscillation is such that the total phase shift is zero (Barkhausen criteria) or the reactances of the inductor and capacitors all cancel out by the following condition

$$\omega_o L - \frac{1}{\omega_o C_0} - \frac{1}{\omega_o C_1} - \frac{1}{\omega_o C_2} = 0. \tag{2.8}$$

The operating frequency is given by the equation

$$\omega_o = \frac{1}{\sqrt{\dfrac{C_0 C_1 C_2 L}{C_0 C_1 + C_0 C_2 + C_1 C_2}}}. \tag{2.9}$$

One of the reasons why *LC* oscillators are used is because they can operate in the GHz range. Op-amp *RC* oscillators can only operate up to tens of MHz [15]. The tuned resonator, consisting of capacitors and an inductor, determines the frequency of *LC* oscillators. The Colpitts/Clapp configuration remains the most popular up to very high frequencies [17] [21]. Microstrip lines can be used to implement the inductor so that the oscillator can operate at higher frequencies without a degradation in Q (i.e. in the tens of GHz range) [22]. The Colpitts structure is difficult to tune over wide frequency ranges compared to the Op-amp *RC* oscillators. This is due to the design limitations of the capacitors, because they have to satisfy (2.5) to maintain oscillation. In the Clapp structure, the extra capacitor C_0 in series with the inductor gives us freedom to tune the frequency, whereas the other capacitors can be used to satisfy the oscillation criteria. This gives an improvement in the tuning range from the Colpitts case. The tuning capacitor C_0 is implemented using trimmer (or variable) capacitors. Voltage dependent variable capacitors (known as varactors) can vary the frequency of oscillation by changing its control voltage [23].

The quality factor Q is related to the oscillation stability, accuracy, and phase noise. The Colpitts/Clapp structure needs a high Q inductor in order to achieve decent phase noise performance [21]. The results of the LTV phase noise model in [16] illustrate that we can achieve minimum phase noise when the active devices remains off almost all the time and wakes up periodically to deliver current at the voltage signal peaks of each cycle. So when this condition is satisfied and we have a high Q, then phase noise would be minimal. The collector current in Colpitts/Clapp oscillator only flows during a short interval that coincides with the peaks of the tank voltage (voltage across the LC network). Therefore the Colpitts/Clapp configuration has excellent phase-noise performance and remains a popular topology [3] [24]. This property will be discussed again in Chapter 5. For a 946 MHz carrier Colpitts oscillator with an off-chip resonator, we get a phase noise of approximately –127 dBc/Hz at a 600 kHz offset from the carrier [25].

Modern set-top DBS TV tuners require high performance (low phase noise and high Q) and low-cost oscillators where the frequency can be controlled by the voltage. Clapp voltage controlled oscillators are used for these TV tuner applications because of its great phase noise performance, voltage-controlled frequency selection and simplistic circuit structure [24].

2.4 5-STAGE RING OSCILLATOR

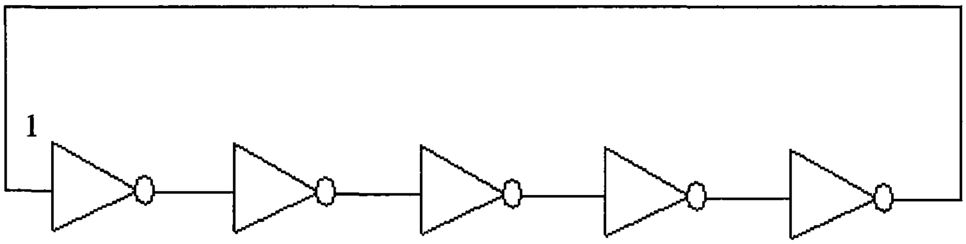

Fig. 2.8: A 5-stage ring oscillator.

To this point, the *LC* oscillator class has been discussed and analyzed. Those oscillators generate continuous analog sinusoidal waveforms with the frequency controlled by the *LC* resonator. The next class of oscillators is known as the ring oscillator. These oscillators are used for digital applications and they generate digital clock pulse signals. Fig. 2.8 depicts a 5-stage ring oscillator. Due to the odd number of inverters in the chain, no stable operation point exists and the circuit oscillates with a frequency of [26]

$$f = \frac{1}{2 \cdot t_p \cdot N} \tag{2.10}$$

where t_p is the propagation delay of the inverter gates and N is the number of gates (five in this case).

This circuit is an astable circuit constantly switching between the “logic-1” and “logic-0” states. Point 1 in the circuit switches from “logic-1” to “logic-0” and back to “logic-1” continuously with a frequency given by equation (2.10). The inverters can be implemented using static CMOS circuits. Gate propagation delay is usually around hundreds of pico seconds, so the frequency for the 5-stage ring oscillator is typically in the 10s of MHz range [26]. From (2.10), the frequency is dependent upon the number of gates and the propagation delay. These values are fixed so the oscillator can not be tuned. However, the ring oscillator can be implemented by using current-starved inverters to replace the regular inverters. The control voltage regulates the propagation delay through the inverter allowing the frequency to be tuned [26].

Ring oscillators are known for their poor phase noise performance. This is because every cycle, the energy stored in node capacitances is reset thereby decreasing Q. The active element restores energy to the circuit during the edge as opposed to the peak of the oscillating output voltage. Recall that the Colpitts oscillator restores the energy during the voltage peaks accounting for its good phase noise performance according to the LTV model for phase noise [16]. Due to the poor Q, the phase noise is unacceptable for RF applications.

In Chapter sections 5.2 , 5.3 and 5.4, the cross-coupled CMOS LC oscillator and the Colpitts oscillator design topologies will be used for the phase noise simulation.

Chapter 3

NOISE SOURCE FROM DEVICE

3.1 INTRODUCTION

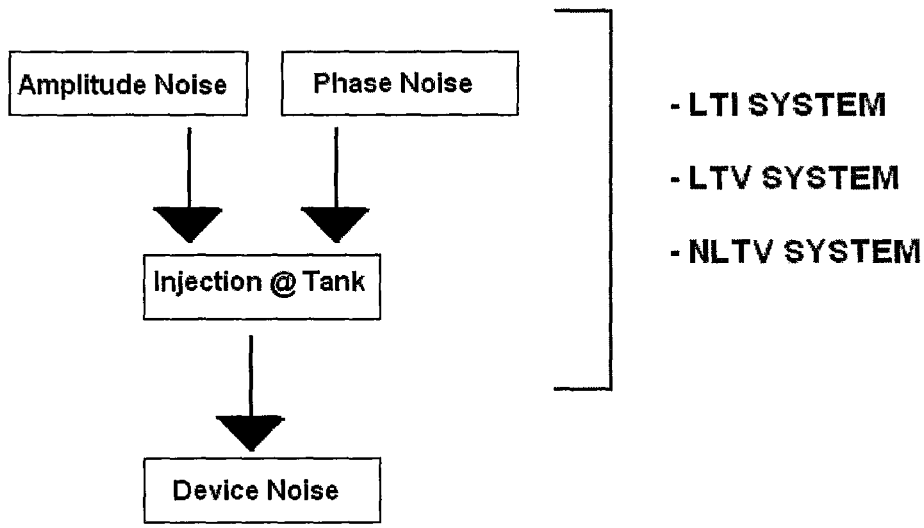

Fig. 3.1: Noise layers.

During an oscillation cycle, noise from the transistors or devices are injected into the oscillator to produce amplitude and phase noise (fig. 3.1). Amplitude noise can be controlled with amplitude-limiting mechanisms so the dominant noise component in oscillators is the phase noise [16]. The different phase noise models (LTI, LTV, and NLTV models) are used to describe the relationship between the input device noise and the output phase noise. Phase noise models are discussed in Chapter 4.

In this chapter, the noise sources from the active devices are discussed extensively. Device noise is the major source of phase noise. These physical noise sources are comprised of two components:

1) the thermal noise in the channel of the MOS transistor
2) the $1/f$ noise

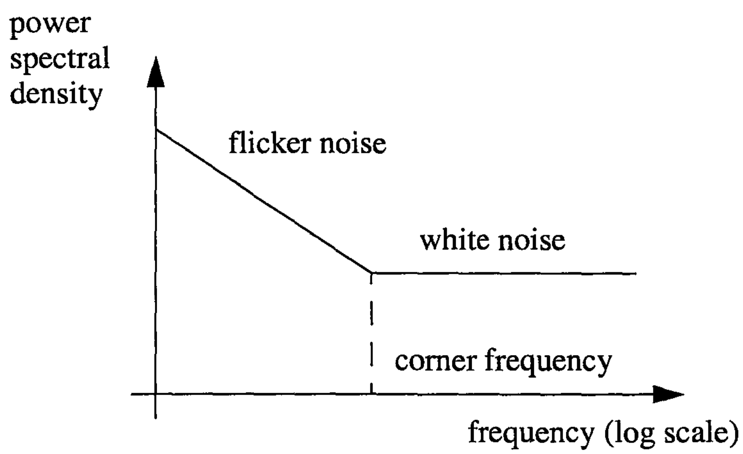

Fig. 3.2: Spectral density of device noise.

The flat portion of the PSD curve in fig. 3.2 is due to the thermal noise and is known as white noise since it is independent of frequency. The sloped region is the $1/f$ noise [27]. For the MOS thermal noise, the standard channel thermal noise model for a MOS transistor is discussed. The $1/f$ noise theories examined include: the mobility fluctuation model due to fundamental scattering processes and the standard carrier density fluctuation model due to traps in the gate oxide.

3.2 THERMAL NOISE

The thermal noise of the MOS transistor affects the phase noise of an *LC* oscillator. This section examines the origins of the thermal noise in the channel of the MOS transistor. When the MOS transistor is operational, there is a resistive channel between the drain and source. In the extreme case when the source is grounded and the drain-source voltage is zero, the channel can be thought as a homogeneous resistor. The thermal noise of the channel is given by

$$i_d^2 = 4kTg \tag{3.1}$$

where g is the channel conductance at zero drain-source voltage, k is the Boltzman's constant and T is the temperature.

When the drain-source voltage is no longer zero, the channel can no longer be considered a homogeneous resistor. The channel must be split into parts of unit length Δx where the thermal noise is applied. Then to calculate the total noise of the channel the thermal noise is integrated over the channel length [28]:

$$i_d^2 = 4kT\frac{\mu^2 W^2}{L^2 I_{DS}}\int_0^{Vds} Q_n^2(V)dV \tag{3.2}$$

where $Q_n(x) = C_{OX}(V_{GS} - V_T(x) - V(x))$, W is the transistor channel width, L is the transistor channel length, V_T is the threshold voltage, C_{ox} is the oxide capacitance, subscripts *GS* is gate to source, subscripts *DS* is drain to source, and μ is the mobility of the carriers. By neglecting the dependency of $V_T(x)$ with position, (3.2) simplifies to [28]:

$$i_d^2(f) = 4kT\mu C_{OX}\frac{W}{L}\frac{2}{3}\left[\frac{3(V_{GS}-V_T)V_{DS}-3(V_{GS}-V_T)^2-V_{DS}^2}{2(V_{GS}-V_T)-V_{DS}}\right]. \tag{3.3}$$

At saturation point ($V_{DS} > V_{GS} - V_T$), (3.3) reduces to [28],[57]:

$$i_d^2(f) = 4kT\mu C_{OX}\frac{2}{3}\frac{W}{L}(V_{GS}-V_T) = 4kT\frac{2}{3}g_m . \tag{3.4}$$

where g_m is the transconductance. Equation (3.4) neglects the body effect in MOS transistors [29]. In reality, the thermal noise is higher due to this body effect because $V_T(x)$ depends on the channel potential. Note that the channel thermal noise is independent of frequency.

3.3 FLICKER NOISE

The major source of phase noise is due to both the 1/*f* noise and thermal noise of the MOS transistor. This section examines the following different 1/*f* noise models: the Mobility Fluctuation (MF) and the Standard Carrier Density Fluctuation (CDF) models. The first model states that the 1/*f* phenomenon is caused by fundamental scattering mechanisms in the MOS system. The second model assumes that the 1/*f* noise is due to the random trappings and de-trappings of mobile carriers by the traps in the gate oxide.

3.3.1 Mobility Fluctuation Model

Flicker or $1/f$ noise is found everywhere in nature but is a severe limitation to analog devices such as voltage-controlled oscillators. The quantum $1/f$ effect arises due to electrical charges in space and time interacting with their field. There are many papers and literature discussing the fundamental quantum $1/f$ noise [31]-[47]. As devices are made smaller, the quantum $1/f$ effect becomes more pronounced. This effect is especially important in nanotechnology [31].

The conventional quantum $1/f$ effect is always present in cross section areas involving current carriers or mobile particles. A physical example of the quantum $1/f$ noise effect is the Coulomb scattering of current carries. Fig. 3.3 illustrates the process of Coulomb scattering. Mobile carriers head in the direction of a fixed immobile charge and as they come within close proximity the electrical forces scatter the carriers in various directions. This fundamental phenomenon produces undesired results (i.e. noise) as it changes the current and mobility characteristics. The scattered electrons are characterized by DeBroglie waves since an electron can be viewed as both a particle and a wave with frequency corresponding to its energy [31]. Some of the electrons have lost energy during the scattering process. Therefore there is a shift in frequency of the DeBroglie waves. Since there are emission of photons at all frequencies, there are probability density fluctuations at all frequencies. The current density fluctuation is found by multiplying the probability density fluctuation with the velocity of the scattered current carriers [31].

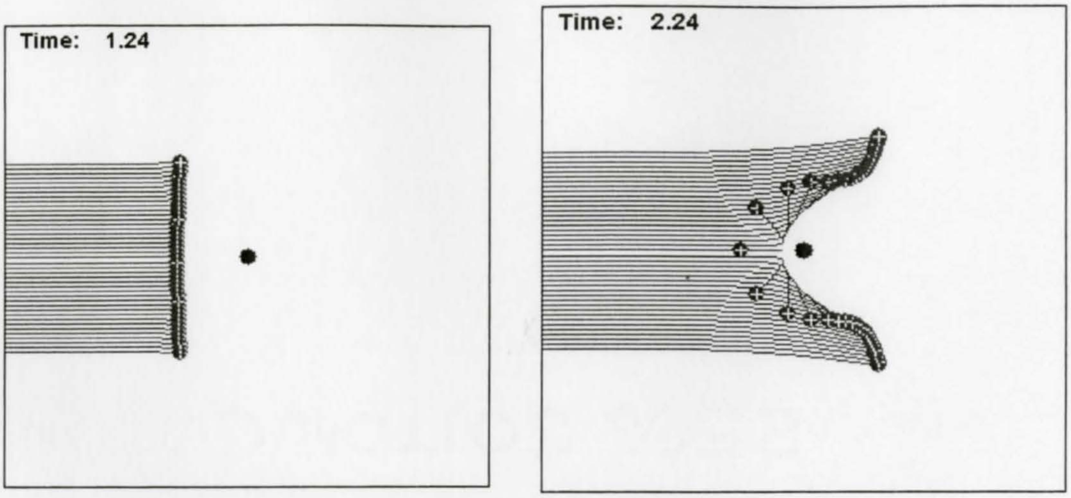

Fig. 3.3: Coulomb scattering [48].

The spectral density for fractional current fluctuation is found to be

$$\frac{i_f^2}{I^2} = \frac{\alpha_H}{fN} \tag{3.5}$$

where α_H is known as the Hooge parameter (empirically derived constant) and N is the number of scattered carriers. Note that the equation is general and can be applied for any type of scattering. Possible scattering processes include impurity scattering (through Coulomb scattering), phonon scattering, and inter-valley scattering [31]. The quantum $1/f$ model can only be applied to homogeneous systems. By applying the quantum $1/f$ noise model to n-channel MOS transistors, we get the starting point for the derivation of the MF model. In the case of the n-channel MOS transistor, the mobile carriers are electrons and the ionized acceptors and fixed charges in the oxide cause impurity scattering.

Since the current has a linear dependence on mobility, the fractional mobility $1/f$ spectral density is also given by (3.5). If there is more than one scattering mechanism involved, Matthiessen's rule can be applied. The Hooge parameter would then be made to incorporate all the scattering processes [31]:

$$\alpha_H = \alpha_l \left(\frac{\mu_{eff}}{\mu_l} \right)^2 \tag{3.6}$$

where the subscript l refers to the event when only lattice scattering is present and the subscript *eff* means effectively taking into consideration all the scattering mechanisms present in the device. α_l is found through experiments and is approximately a constant value of 2×10^{-3} at room temperature for MOS transistors [28]. The fact that the Hooge parameter is a constant indicates that the quantum $1/f$ noise is a fundamental phenomenon.

When $V_{DS} << V_{SAT} = V_{GS} - V_T$, the n-channel MOS transistor is said to be operating in the linear region. Under strong inversion in the linear region, the total number of carriers N in the inversion channel is given by the equation [29]

$$qN = C_{ox}WL(V_{GS} - V_T)\,. \tag{3.7}$$

For small V_{DS}, the drain source current is given by the equation [28],[57]

$$I_{DS} = \frac{q\mu_{eff} N}{L^2} V_{DS}\,. \tag{3.8}$$

The Hooge equation (quantum $1/f$ model) can be used because the channel can be considered homogeneous. Using the above equations, we have the following current spectral density when the MOS transistor is in the linear region:

$$i_f^2 = \alpha_H \frac{q\mu_{eff} I_{DS} V_{DS}}{L^2 f} . \tag{3.9}$$

When $V_{DS} = V_{SAT} = V_{GS} - V_T$ (ignoring channel length modulation), the MOS n-channel transistor is operating in the saturation region for strong inversion channels [29]. In this case, the channel is no longer homogeneous and we must consider small sections Δx along the channel to apply the Hooge equation. Then the total $1/f$ noise spectrum can be obtained by integrating over the whole channel for MOS transistor in saturation region [29]:

$$i_f^2 = \alpha_l \frac{q\mu_f (V_{GS} - V_T) I_{DS}}{L^2 f} . \tag{3.10}$$

where μ_f incorporates the effect mobility of electrons over the whole channel. The transconductance of the MOS transistor is given by the equation [29]

$$g_m = \sqrt{2\mu_{eff} C_{OX} \frac{W}{L} I_{DS}} . \tag{3.11}$$

By dividing the square of (3.11) to (3.10), the equivalent input 1/f noise voltage spectrum at the gate can be found [28],[57]:

$$v_g^2 = \alpha_l \frac{q\mu_f (V_{GS} - V_T)}{2\mu_{eff} C_{OX} WLf}. \tag{3.12}$$

Thus the $1/f$ gate voltage noise described by the MF model is given by (3.12) where the noise is proportional to the gate voltage provided the two mobility variables are independent of the gate voltage. This result can be explained intuitively: as the gate voltage is raised, more electrons are attracted towards the surface along the channel. As the carriers are increased, there will be more collisions due to scattering and hence more noise. When the gate voltage is raised even further, the electrons may be pulled towards the oxide where scattering with the fixed charges in the oxide may further increase the noise. As mentioned, the $1/f$ nature of the noise is due to particle-wave quantum nature of electrons. The MF model for $1/f$ noise (3.12) is proportional to the thickness of the oxide and temperature through the oxide capacitance and threshold voltage. It is also proportional to the DC gate bias. We will see shortly that the next $1/f$ model discussed has a gate voltage spectral density that is independent of the DC gate bias.

3.3.2 Standard Carrier Density Fluctuation Model

The MF model explained the $1/f$ noise phenomenon through fundamental scattering mechanisms of the mobile carries in the MOS channel. The Carrier Density Fluctuation (CDF) model uses a different approach: it states that the $1/f$ noise is caused by the random trappings and de-trappings of mobile carriers by traps located at the Silicon-Oxide interface [28]. Instead of using the quantum wave nature of electrons to attain the noise frequency characteristic, this model treats the carriers as particles and relates the noise frequency behavior through the trap capture and emission rates. This is the key difference in philosophy taken by the MF and CDF models.

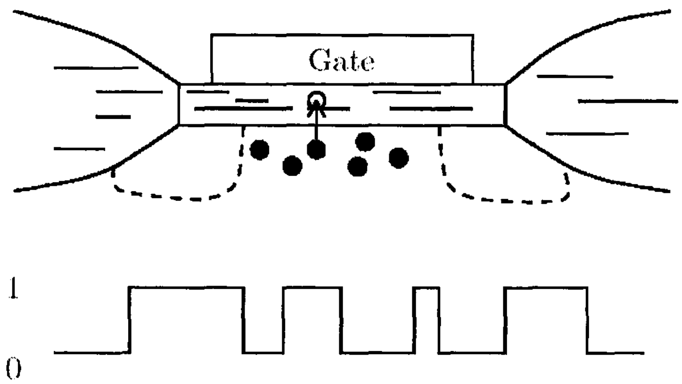

Fig. 3.4: Single trap in MOS gate oxide and corresponding trapped electron number [49].

The top figure in fig. 3.4 illustrates a single trap in the gate oxide of a MOS transistor. The oxide trap can capture channel carries in proximity or release previously captured carriers. The bottom figure in fig. 3.4 shows the fluctuations in the state of the trap ("1" corresponds to a filled trap and "0" corresponds to an empty trap). Fig. 3.5 depicts the energy band diagram of the system. The dashed lines indicate when the transistor is "on" ($V_{GS} > V_T$) and the solid lines are when the transistor is "off". E_t is the energy level of the trap in the oxide and E_F is the Fermi level of the bulk semiconductor.

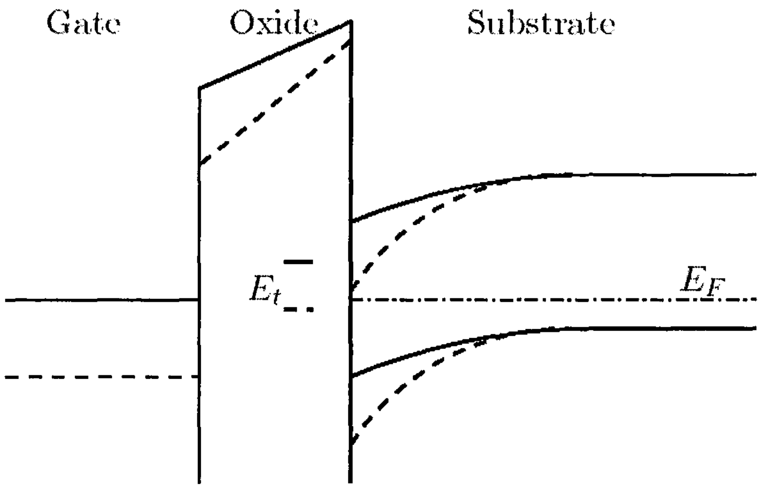

Fig. 3.5: Energy band diagram of a MOSFET [49].

The energy states along the interface interact with the traps in the oxide randomly through the free charges in the channel. These electrical interactions obey the Shockley Read Hall statistics and the resulting mean square fluctuation of the number of trapped carriers in a unit volume ΔV at a specific position is given by the equation [28]

$$\partial n_t = \frac{4\tau}{1+w^2\tau^2} N_t f_t (1-f_t)\Delta V \tag{3.13}$$

where $f_t = \dfrac{1}{1+e^{\frac{E_t - F_t}{kT}}}$. τ is defined as the trapping time constant, N_t is the density of traps in the oxide, f_t is the fraction of filled traps in steady state, E_t is the trap energy level and F_t is the trap quasi-Fermi level. Notice that (3.13) is a function of frequency ("1/f" nature) where the frequency nature is due to the trap rates. The fluctuation of the trapped carrier number ∂n_t causes fluctuations in the channel free carrier ∂N which in turn causes fluctuations in the drain-source current [28].

We will now assume that the MOS transistor is in strong inversion. The 1/*f* model proposed in [50], "General Inversion Carrier Density Fluctuation Model", corrects Assumption A and allows for any type of inversion. However the standard CDF model assumes that the MOS transistor is in strong inversion. If this is the case, the following holds [28],[57]:

$$\partial N \approx \partial n_t . \tag{3.14}$$

Equation (3.14) states that the channel carrier fluctuation is approximately equivalent to the fluctuations in the number of trapped carriers in the oxide trap. In strong inversion, it can be approximated that the electrons being trapped are taken from the large repository of carriers in the channel.

The fluctuation in the drain current due to fluctuations in trapped carriers in unit volume ΔV at a given position along the channel x is given by the equation [28]

$$\partial i_d^2(f) = \left(\frac{I_{DS}}{Ln(x)} \right)^2 \partial N^2 . \tag{3.15}$$

Assuming the charge sheet model for the MOS channel [29], the number of free carriers $n(x)$ in the channel at a position x (recall that strong inversion is being assumed) is given by equation [29]

$$n(x) = WC_{OX}(V_{GS} - V_T - V(x)). \tag{3.16}$$

Since the MOS is in strong inversion, the current is approximately due to drift current [28]:

$$I_{DS} = qn(x)\mu \frac{dV(x)}{dx}. \tag{3.17}$$

Combining the above equations and integrating along the channel position x, over the energy band-gap for the trap energy level and into the oxide, we get the following [29]:

$$i_d^2(f) = \int_0^{V_{DS}} \int_{E_v}^{E_c} \int_0^d \frac{\mu q^2 I_{DS}}{L^2 C_{ox}(V_{SAT} - V(x)} \frac{4\tau(y,E,V)}{1 + w^2\tau^2(y,E,V)} N_t(E,y) f_t(E,V)(1 - f_t(E,V)) dydEdV . \tag{3.18}$$

Equation (3.18) is integrating over the depth into the oxide y (where the trap density and trap time constant is dependent on), the energy level between the valance and conduction band of the semiconductor to cover all the trap energy levels, and across the channel position where the voltage along the channel varies. Before the integration of (3.18) is performed, few assumptions will be made to simplify this procedure.

Another assumption is made in the model derivation: the traps are uniformly distributed into the oxide. Thus, the oxide trap density $N_t(E,y)$ is independent of the oxide depth y. The distribution of the trap time constant $\tau(y,E,V)$ into the oxide obeys the SRH statistics and the McWhorter Tunneling model [28],[57]:

$$\tau(y) = \frac{1}{c(n_s + n_l)} e^{\alpha y}. \tag{3.19}$$

The parameters are the McWhorter Tunneling constant $\alpha = 10^8$ cm and electron capture coefficient $c = 10^{-8}\, cm^3 / s$. The surface carrier concentration is given by [29]:

$$n_s = n_i e^{(F_n - E_i)/kT} \tag{3.20}$$

where F_n is the bulk quasi-Fermi level and E_i is the silicon intrinsic Fermi level. The concentration of trapped electrons is given by [29]:

$$n_l = n_i e^{(F_t - E_i)/kT}. \tag{3.21}$$

Due to the second assumption, the resulting noise spectrum will show the $1/f$ behavior. When the traps are not uniformly distributed, the noise spectrum will exhibit the $1/f^{\eta}$ characteristic.

The third assumption is made regarding the trap distribution which assumes that only traps near the electron quasi-Fermi level are effective in noise generation. Thus, the following approximation from variables that are functions of energy level in (38) is made [28],[57]:

$$N_t(E, y) f_t(E, V)(1 - f_t(E, V)) \approx N_t(F_n) f_t(F_n, V)(1 - f_t(F_n, V)). \tag{3.22}$$

Using SRH statistics, the following holds [28],[57]:

$$f_t(F_n,V)(1-f_t(F_n,V))=\frac{n_s^4}{(2n_x^2+n_i^2)^2}. \tag{3.23}$$

Equation (3.23) states that we only care about the trap levels at the Fermi-level of the semiconductor. Therefore we have the following:

$$E_t \approx F_n\,. \tag{3.24}$$

From fig. 3.5, (3.24) is valid when the transistor is turned on (dashed-lines in the figure). But when the transistor is turned off, this is no longer valid. The voltage along the channel varies with x so the surface density of electron carriers changes with x. The change in the surface potential of the silicon across the channel is exponential with the position x and is given by the equation [28]

$$V_{GB}(\Psi_s)=V_{FB}+\Psi_s+\gamma\left(\sqrt{\Psi_s+\phi_t+e^{(\Psi_s-(2\phi_f+V_{CB}))/\phi_t}}\right) \tag{3.25}$$

where Ψ_s is the Si potential and V_{CB} is the channel potential.

Finally, the last assumption is that the silicon channel potential and the surface density of the electrons in the channel is linear across the channel. With this assumption, the following simplification holds [28],[57]:

$$n_s=n_{so}\frac{V_{SAT}-V(x)}{V_{SAT}} \tag{3.26}$$

where n_{so} is the surface electron density at the source when it is ground.

Now we can evaluate the integral in (3.18) which yields [28],[57]:

$$i_d^2(f) = \frac{\mu q^2 I_{DS} ktN_t}{16L^2 C_{OX} \alpha f} \ln\left[\frac{2}{2\left(\frac{V_{SAT} - V_{DS}}{V_{SAT}}\right)^2 + \left(\frac{n_i}{n_{so}}\right)^2}\right]. \tag{3.27}$$

Equation (3.27) is valid up into the saturation point. After this point, there is channel length modulation and the pinch-off point shifts closer towards the source and (3.27) is no longer valid and the length of the effective channel L will decrease. If the transistor is well below the saturation point ($V_{DS} << V_{SAT}$) and in strong inversion, (3.27) can be modified to the following equation [28],[57]

$$i_d^2(f) = \frac{\mu q^2 I_{DS} ktN_t}{16L^2 C_{OX} \alpha f} \ln\left[\frac{\sqrt{2} n_{so}}{n_i}\right] = \frac{K_F I_{DS}}{C_{OX} L^2 f}. \tag{3.28}$$

Unlike the MF model, the standard CDF model is proportional to the squared of the oxide thickness (instead of the oxide thickness itself) and is independent of the DC gate bias. Both models do not take into account the channel length modulation that occurs after the saturation point. Using each of these $1/f$ models will provide different results for the $1/f$-induced phase noise of an oscillator. Table 1 shows the $1/f$ noise models. The first two entries correspond to the two $1/f$ models discussed previously. The non-uniform trap density CDF model proposed in [51] corrects the second assumption by noting that the traps are not uniformly distributed in the oxide and the noise does not exactly follow the $1/f$ noise characteristic. The MF and non-Uniform trap CDF models will be used in Chapter 5.5 for phase fluctuation simulation.

TABLE 3.1. Flicker Noise Models

1/*f* noise models	1/f Noise Equations	Operating Region	Assumptions and Limitations	Key Parameter Dependencies
MF Model [28],[57]	$v_g^2(f) = \alpha_l \dfrac{q\mu_f (V_{GS} - V_T)}{2\mu_{eff} C_{OX} WLf}$	Strong inversion, saturation	Works only for homogeneous devices	- depends on gate bias - proportional to oxide thickness and temperature
Standard CDF Model [28],[57]	$v_g^2(f) = \dfrac{K_f(T)}{C_{OX}^2 WLf}$	Strong inversion, linear	- Assumes uniform trap density - Assumes trap energy level independent of gate bias	- proportional to squared of the oxide thickness and temperature
Non-Uniform Trap Density CDF Model [51]	$v_g^2(f) = \dfrac{K_{non-uniform}(T)}{C_{OX}^2 WLf^{\eta}}$	Strong inversion, linear	Assumes trap energy level independent of gate bias	- the η parameter effects the 1/*f* noise characteristic - -proportional to the squared of the oxide thickness and temperature

Chapter 4

PHASE NOISE THEORIES & IMPLEMENTATIONS

4.1 LTI LEESON-CUTLER PHASE NOISE THEORY

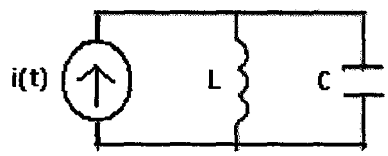

$$i(f) \xrightarrow{LTI} v_n(f)$$

Fig. 4.1: LTI phase noise system.

This section examines the Leeson-Cutler Linear Time Invariant (LTI) model for phase noise. Consider fig. 4.1 where the current source is the input noise (due to device or thermal noise) and the transistors provide negative resistance that effectively cancels out the physical parasitic resistance of the *LC* network. Thus we are left with a noise current source and a parallel *LC* network. The LTI phase noise model describes the input as device noise current $i_n(f)$ and the output as the voltage fluctuation $v_n(f)$ due to the input. The relationship between the input and the output is linear time invariant.

The parallel impedance looking into the LC network is given by the following:

$$Z = \frac{j\omega L}{1-\omega^2 LC} = \frac{j\omega L}{1-\omega^2 LC}. \tag{4.1}$$

Letting $\omega = \omega_o + \Delta\omega$ where $\omega_o = \frac{1}{\sqrt{LC}}$ is the natural frequency of the LC network and $\Delta\omega$ is the offset from the natural frequency, we have [16]:

$$Z = \frac{j\omega_o L + j\Delta\omega L}{-2w_o \Delta w LC + \Delta w^2 LC}. \tag{4.2}$$

$$Z \approx \frac{j\omega_o L}{2((\Delta\omega)/\omega_o)} \tag{4.3}$$

where $\Delta\omega \ll \omega_o$ is assumed. Equation (4.3) assumes that the offset frequency is much smaller than the natural or carrier frequency. Thus we are only considering the noise that is close to the natural frequency of the oscillator.

The quality factor Q is defined as the energy stored divided by the energy dissipated in the resonator [16]:

$$Q = \frac{E_{stored}}{E_{diss}} = \frac{\omega_o E_{stored}}{P_{diss}} = \frac{\frac{1}{2}(\omega_o C V_{pk}^2)}{\frac{1}{2}\left(\frac{V_{pk}^2}{R}\right)} = \frac{R}{\omega_o L} \tag{4.4}$$

where R is the parallel equivalent resistance of the LC network. Using (4.3), the magnitude of the impedance Z is given by the equation [16]

$$|Z| = R\frac{\omega_o}{2Q\Delta\omega}. \tag{4.5}$$

Using (4.5), the output voltage noise spectral density of the LC oscillator is given below where $\frac{i^2}{\Delta f}$ is the input noise current spectral density [16]:

$$\frac{v_n^2}{\Delta f} = \frac{i^2}{\Delta f}|Z|^2 = \frac{i^2}{\Delta f}\left(\frac{R \cdot \omega_o}{2Q\Delta\omega}\right)^2. \tag{4.6}$$

The Equipartition Theorem of Thermodynamics states that in equilibrium the amplitude and phase noise powers is equivalent [16]. Thus the phase noise spectral density is half of the spectral density in (4.6). The phase noise is characterized by the following equation, which measures the power of the sideband at a frequency offset due to noise relative to the power of the carrier at a unit bandwidth [16]:

$$L\{\Delta\omega\} = 10\cdot\log\left(\frac{P_{SB}(\omega_o + \Delta w, 1Hz)}{P_{carrier}}\right) = 10\cdot\log\left(\frac{\frac{1}{2}\frac{v_n^2}{\Delta f}}{\frac{1}{2}v_{pk}^2}\right) = 10\cdot\log\left(\frac{i^2}{\Delta f}\left(\frac{\omega_o}{2Q\Delta\omega}\right)^2\frac{R}{2P_{sig}}\right) \quad (4.7)$$

where P_{sig} is the power of the oscillator or carrier signal and Q is the quality factor of the resonator. The input current noise term $\frac{i^2}{\Delta f}$ in (4.7) can be due to the $1/f$ and thermal noise of the device or LC network. The method used to derive (4.7) is the LTI approach: it does not take into account the time-varying nature of the oscillator phase noise system. Note that (4.7) becomes invalid when the offset frequency becomes too large. Thus this model is only valid for noise that have frequencies very close to the natural frequency of the LC oscillator.

For input current noise due to the thermal noise, (4.7) becomes:

$$L\{\Delta\omega\} = 10\cdot\log\left(\frac{i^2}{\Delta f}\left(\frac{\omega_o}{2Q\Delta\omega}\right)^2\frac{R}{2P_{sig}}\right) = 10\cdot\log\left(\frac{2kT}{P_{sig}}\left(\frac{\omega_o}{2Q\Delta\omega}\right)^2\right). \quad (4.8)$$

Note that (4.8) neglects the flicker noise contribution from the device. The units of phase noise are dBc/Hz at a particular frequency offset from the carrier.

The Leeson-Cutler model is a modification of (4.8) that is semi-empirical and takes into account the flicker noise and noise floor regions where F is a fitting parameter and $\Delta\omega_{(1/f)^3}$ is the corner frequency between the $1/f^3$ and $1/f^2$ regions discussed next [16]:

$$L\{\Delta\omega\} = 10 \cdot \log\left(\frac{2FkT}{P_{sig}}\left[\left(1+\frac{\omega_o}{2Q\Delta\omega}\right)\right]^2\left(1+\frac{\Delta\omega_{(1/f)^3}}{|\Delta\omega|}\right)\right). \tag{4.9}$$

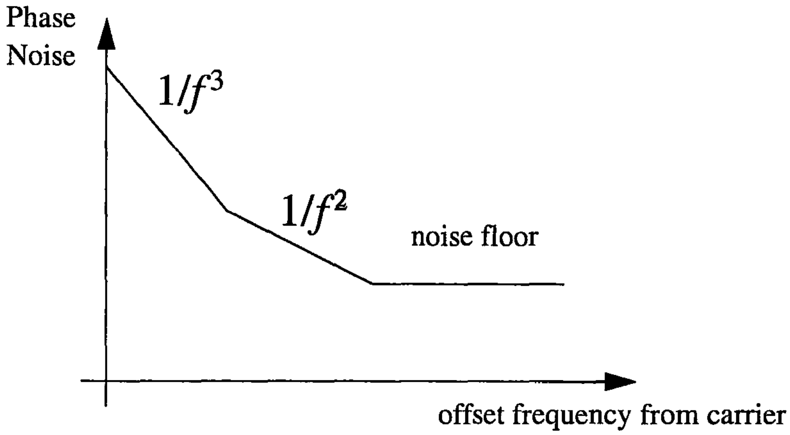

Fig. 4.2: Typical plot of phase noise in an oscillator [3].

Fig. 4.2 shows the plot of the phase noise from the empirical equation (4.9). The horizontal axis is the offset frequency from the carrier or oscillation frequency. If the oscillator had no phase noise, there will be an impulse peak in the power spectrum at the carrier frequency because of the sinusoidal voltage waveform. But due to phase noise, there are side-band noise at frequencies away from the carrier frequency as shown in fig. 4.2. The phase noise graph measures the power of the side-band noise (at a certain offset frequency from the carrier frequency) relative to the power at the carrier frequency. The flicker noise contributes to the $1/f^3$ region while the thermal noise dominates the $1/f^2$ region in fig. 4.2. The low frequency phase noise is characterized by the $1/f^3$ region up until the corner frequency where the $1/f^2$ region starts to dominate. As the frequency deviation from the natural oscillator frequency becomes large enough, the flat-band region known as the noise floor begins to dominate. The noise floor is caused by the output amplifier in the oscillator.

4.2 LTV PHASE NOISE THEORY

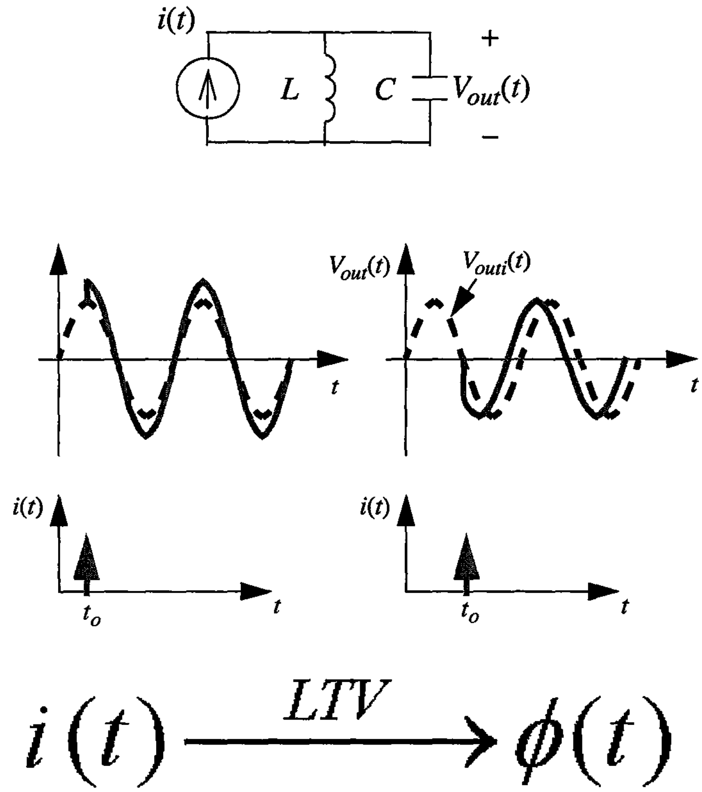

Fig. 4.3: LTV phase noise system.

In the previous section the phase noise system was assumed to be LTI. This section examines the phase noise theory proposed in [5] that takes into account the time-varying nature of the phase noise system. The input into the system is the device noise current and the output is the phase fluctuation in the time domain. This model assumes a linear and time varying relationship between the input and the output. In fig. 4.3, an impulse noise current is injected into the *LC* oscillator system. In the first case the noise current is being injected when the oscillator voltage waveform is at the maximum amplitude (dashed curve). Instead of the resulting waveform being phase-shifted, the waveform retains its phase characteristics but with an increase in amplitude due to the injection (solid curve). This corresponds to zero phase disturbance or noise. Contrast this scenario with the second case where the noise injection occurs when the voltage waveform is at the zero-crossing point (dashed curve). In this case, the amplitude of the waveform remains constant but the phase of the resulting waveform is changed (solid curve). This phase fluctuation contributes to the phase noise of the oscillator. So intuitively, we can see that the phase noise system is time-varying implying that the phase error of the resulting waveform is dependent on when the impulse noise current is injected. This approach characterizes the impulse response of the phase noise system.

The time varying characteristics can be shown in the limit cycle graph in fig. 4.4. The horizontal axis is the oscillator voltage and the vertical axis is its derivative. Point A corresponds to the peak of the waveform, point B is the zero-crossing point and point C is a point between A and B. When we inject a noise current, there is voltage fluctuation due to the excess charge. Injection at point C in the limit cycle causes a change in both voltage amplitude and phase (angle between the positive voltage axis and vector C) as shown in the figure. However when we inject at point A there is only a change in amplitude and the phase remains unchanged. Injection at point B yields maximum phase change but without any amplitude fluctuation since the slope of the circular curve is zero relative to the horizontal voltage axis. The relationship between the phase change and the injected noise current is non-linear. However the LTV model assumes a linear relationship between these two components.

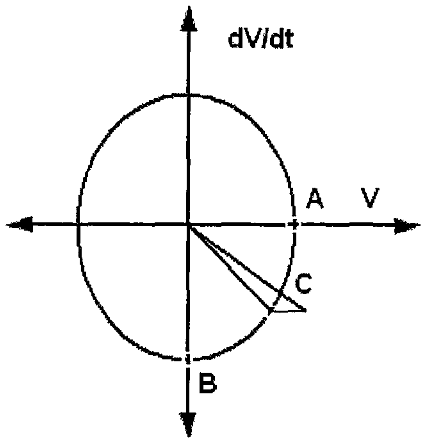

Fig. 4.4: Limit cycle.

This time-varying property is captured by the following LTV equation describing the phase fluctuation in the time domain due to current noise injection i [5]:

$$\phi(t) = \int_{-\infty}^{\infty} h(t,\tau) i(\tau) d\tau = \frac{1}{q} \int_{-\infty}^{t} \Gamma(\omega\tau) i(\tau) d\tau \qquad (4.10)$$

where $h(t,\tau)$ is the time-varying phase noise transfer function described by the maximum charge on the node q and the unit-less Impulse Sensitivity Function (ISF) $\Gamma(\omega\tau)$. Note that the current-to-phase transfer function is assumed to be linear. This equation adds up all the phase shifts in the past (before time t) due to each noise injection. The ISF acts as a weighting factor for each noise injection taking into account the time varying properties of the system illustrated in fig. 4.3. It notes when each noise injection was injected and calculates the corresponding phase shift factor. It should be noted that the LTV model describes the time-domain phase fluctuation that causes phase noise as due to the total integrated phase shift at the present time. The NLTV model discussed in the next section views the phase fluctuation leading to phase noise in a different way.

The ISF characterizes how sensitive an oscillator is to phase fluctuation due to impulse noise injection and is unique for each oscillator topology. Fig. 4.5 shows the ISF waveforms for an LC oscillator and a ring oscillator. The ISF is at its peak when the oscillator waveform is at its zero-crossing point (maximum phase variation). When the oscillator waveform is at its peak, the ISF is at the zero-crossing point (minimum phase variation). When the input noise current is injected into the system when the oscillator waveform is at the zero-crossing point, the ISF outputs a maximum value leading to maximum phase variation. We have no phase variation and zero ISF point when the noise current is injected at the peak point of the oscillator waveform. The ISF is periodic in nature and its shape depends on the particular oscillator topology. Voltage modulation is performed to convert the phase fluctuation in the time domain given by (4.10) to a voltage fluctuation by using the original oscillator voltage equation:

$$V(t) = A \cdot \cos(\omega t + \phi(t)) \tag{4.11}$$

where A is the amplitude of the voltage waveform.

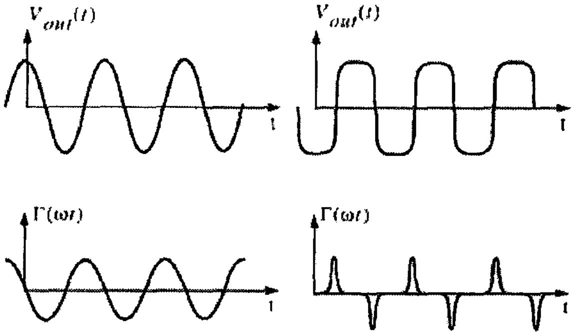

Fig. 4.5: ISF for an LC oscillator (left) and a ring oscillator (right) [5].

The Fourier Transform is used to convert the voltage fluctuation to the frequency domain. With the voltage spectrum we can calculate the phase noise power by the following equation [5]:

$$L\{\Delta\omega\} = 10 \cdot \log\left(\frac{P_{SB}(\omega_o + \Delta w, 1Hz)}{P_{carrier}}\right). \tag{4.12}$$

The flicker and thermal noise define the shape of the resulting phase noise graph. Fig. 4.2 shows the phase noise graph due to the $1/f$ and thermal noise injections. The flicker noise contributes to the $1/f^3$ region while the thermal noise creates the $1/f^2$ region. The LTV model predicts that the corner frequency of the device it not necessarily same as the $1/f^3$ corner frequency assumed by the LTI model. In the next section we introduce the NLTV phase noise model which is an extension of the LTV model.

4.3 NLTV MEMORY THEORY

Consider fig. 4.6 depicting the oscillator output waveform and its corresponding ISF function. As discussed before, the ISF at its peak points implies the time in which the oscillator is most sensitive to noise injection (i.e. greater phase noise). One of the peak points is circled in fig. 4.6 and labelled as the -180-degree point. The ISF near the zero crossing point implies the time of lower sensitivity to noise injection (i.e. low phase noise) and is labelled in the graph as the 10 degree point.

Consider two impulse injections, one at the -180-degree point and the other further down the timeline at the 10-degree point. The first injection point is such that an injection at that point yields a -180 degrees phase change. The second injection point implies a phase change of 10 degrees. If the LTV phase noise model (4.10) is used, the first phase shift is -180 degrees and the second one +10 degrees giving a total phase shift of -180 + 10 = -170 degrees. The LTV model simply adds up all the phase shifts given by the ISF curve corresponding to the impulse injection points.

However phase has the memory property. Consider again the two impulse injections where the first noise injection is at the -180-degree point. After the first noise injection, the oscillator and ISF waveforms are shifted by -180 degrees. The second injection point is then found to have a phase shift of -10 degrees instead of the +10 degrees in the LTV model case. It must be remembered that phase changes are permanent and will always remain in the system. The phase change caused by the first injection remains in the phase noise system indefinitely. So we must shift the ISF curve before the processing of the second impulse injection.

We can define the **memory property** by the following statement: the phase noise system possesses the memory property if after each and every noise injection the oscillator waveform and its ISF are shifted by the phase change due to the injection.

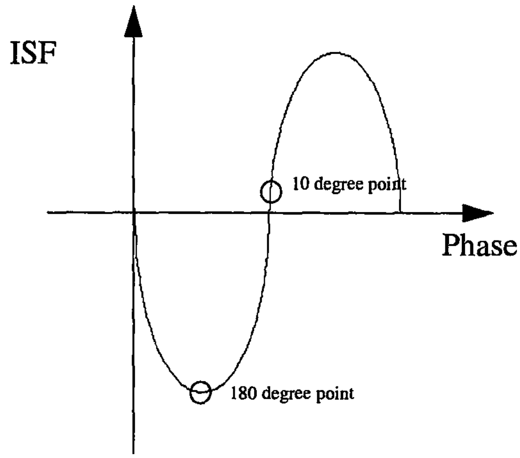

Fig. 4.6: Memory property ISF curve example.

The algorithm for calculating phase fluctuation in the time domain using the memory property is referred to as the Non-Linear Time Varying (NLTV) model and is shown below:

$$\begin{aligned} &if \quad i(\tau_i) \neq 0 \quad then \quad \phi_{i+1} = \frac{1}{q}\Gamma(\omega\tau_i + \phi_i)i(\tau_i) \\ &else \quad \phi_{i+1} = 0 \end{aligned} \tag{4.13}$$

The input noise current is first broken up into discrete impulses or sampled values. At a particular time t, if there is no noise injection (i.e. the input noise current is zero at time t) then the phase fluctuation is zero. If there is noise injection at time t, the following occurs:

1) phase shift by the amount of the previous noise injection

2) compute the new phase shift from the current noise injection

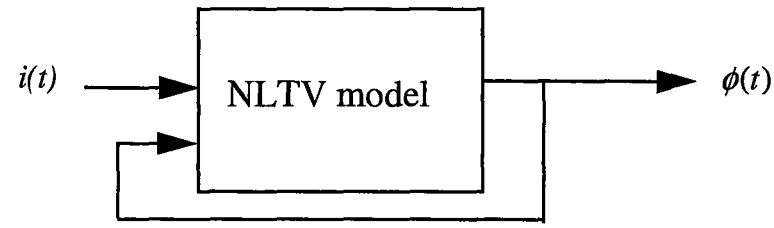

Fig. 4.7: NLTV phase noise system.

It should be noted that the NLTV model (4.13) is linear when the input noise current is a single impulse. Thus for single impulse injections at one point in time, the NLTV model (4.13) simplifies to the LTV model (4.10). In the general case for noise injections at multiple points in time, the system is non-linear. This is because the algorithm (4.13) is recursive and the relationship between the output phase fluctuation and the input current is non-linear. Fig. 4.7 depicts the recursive NLTV phase noise system showing the relationship between the input noise current and the output phase fluctuation.

In the LTV model, the phase fluctuation (4.10) that causes phase noise (4.12) is the total integrated phase shifts from the previous noise injections. In the NLTV model, the phase fluctuation leading to phase noise is the current phase shift the oscillator experiences as opposed to the total integrated phase shifts. The difference between the two views will be discussed in Chapter 5.2. Being an extension of the LTV model, the NLTV model also incorporates the time-varying property through the ISF. It is a more general model of phase noise since it takes into account the permanent phase changes caused by injections at multiple time points.

4.4 DRP METHODOLOGY

The Discrete Recursive Procedure (DRP) is developed to implement the NLTV model algorithm (4.13) and to provide a systematic guideline to calculate phase noise. It uses concepts from the LTV phase noise theory and derives the phase noise for any given input noise injection and oscillator topology. The discrete time domain is used for the all variables and vectors in the phase noise computation. The Fast Fourier Transform (FFT) is utilized for frequency domain transformation.

The six steps of the DRP for phase noise calculation are:

1) Circuit (CAD) Simulation for ISF Sensitivity Waveform and accompanying Cyclostationary effects
2) Noise Calculation & Parameter Input
3) Fourier Series Fitting for ISF Function
4) Noise Integration in Time Domain
5) Phase Fluctuation Computation using the NLTV or LTV models
6) Voltage Modulation and Phase Noise Calculation

In the first step, CAD simulation is used to find the ISF waveform for a particular oscillator topology. Recall that the ISF waveform is used to capture the time-varying phase noise property of the particular oscillator topology. Impulses are injected at eight time points within an oscillation cycle and the voltage points are recorded after some time t_1 for each of the injections. Each of these voltage readings corresponds to a particular phase shift in the original unperturbed waveform. The phase shifts are used to estimate the 8-point ISF. Since the noise injection contains a finite time width and current value (Amps/second), the ISF is normalized by the total amount of charge injected into the circuit. Since the source of noise originates from the transistors and the transistor current changes periodically, the noise should also change with the current. Noise is minimal when the device is off and maximum during a current peak. Thus the device noise is said to be a cyclostationary noise source [5],[52]. The cyclostationary properties of noise is reflected in the cyclostationary waveform. Transient analysis in the CAD simulator is performed to find the cyclostationary waveform that is weighted against the ISF to produce an effective ISF [5].

In the second step, calculation for noise is performed. Sinusoidal injections with varying frequencies but constant amplitudes are a representation of thermal noise in the time domain. Parameters such as voltage swing, time step, number of periods, FFT parameters and oscillation frequency are input into the system. The third step involves approximating the 8-point ISF data by a closed-form mathematical equation using nth-order Fourier series fitting approximation. A closed-form ISF equation is needed for the NLTV algorithm (4.13). The Matlab Curve Fitting (CF) tool (*cftool* function) is used to implement the Fourier series fitting. The ISF data points are extended periodically and processed by the CF tool. There are several different types of fits available including the Fourier series, polynomial, and exponential fits. The Fourier series fitting is used to fit sinusoidal data points. The tool computes the fit and shows the coefficient bounds and the accuracy statistics for the fit. The confidence bounds define the upper and lower limits of the fitted coefficients. The interval width is the distance between the upper and lower limits. By default 90% confidence bounds are calculated suggesting that there is 90% probability that new observation is contained within the bounds or interval. When the interval width is wide more data points should be used to achieve a more accurate and closely bounded fit. The root mean square error (RMSE) is known as the fit standard error and should be close to zero for acceptable approximation [59].

In the forth step, a frequency sweep is performed for noise injection. The thermal and flicker noise are combined into a single noise source in the time domain and input into the system. This is realized by the integration of the frequency-varying sinusoidal waveforms in the time domain. The thermal and flicker noise sources are treated as time-domain deterministic signals. Using either the LTV model (4.10) or the NLTV model (4.13), we can perform the phase fluctuation computation in the time domain. For the NLTV model, the closed-form nth order Fourier Series fitting ISF equation is used. Voltage modulation for conversion into the voltage domain and its resulting phase noise calculation is performed in step six. With the phase noise results, a comparison can be made between the two models. As will be shown in the next chapter, there is a significant difference in phase noise between both models for a special case.

The greater the phase fluctuation in the time domain implies more phase noise. When making phase noise comparisons, the reason that a certain model has greater phase noise performance implies that its phase fluctuation is lower. This will be shown in the next chapter.

4.5 FAST FOURIER TRANSFORM (FFT) ANALYSIS

The Discrete Fourier Transform (DFT) converts a discrete signal in the time domain to a discrete signal in the discrete frequency domain. The Discrete Fourier transform formula is shown below [58],[60]:

$$y_k = \sum_{j=0}^{n-1} a_j (w_n^k)^j \tag{4.14}$$

where $k = 0,1,2,\ldots, n-1$, the vector y with length n is the DFT of the vector a of length n and $w_n^k = e^{-(j2\pi k)/n}$ are the n complex nth roots of unity. In general, the DFT can be computed in $O(n^2)$ time [58].

The Fast Fourier Transform (FFT) is a special case of the DFT. It was developed by J. Tukey and J. Cooley [61] to reduce the number of computations to $O(n \log n)$ time [58]. The FFT method uses a divide-and-conquer strategy by separating the polynomial to an even-index coefficient and odd-index coefficient based $n/2$ polynomials (the Tukey-Cooley decomposition) [58],[61]:

$$A^{[0]}(x) = a_0 + a_2 x + a_4 x^2 + \ldots + a_{n-2} x^{n/2-1}, \tag{4.15}$$

$$A^{[1]}(x) = a_1 + a_3 x + a_5 x^2 + \ldots + a_{n-1} x^{n/2-1}. \tag{4.16}$$

Using (4.15) and (4.16), we have the following equation [58],[61]:

$$y_k = A^{[0]}((w_n^k)^2) + (w_n^k)^2 \cdot A^{[1]}((w_n^k)^2)\,. \tag{4.17}$$

The sub-problems (4.15) and (4.16) have the same form as the original problem (4.14) but are now half the size. The original n-element DFT computation is divided into two $n/2$-element DFT computations. The FFT algorithm is a recursive procedure that implements equation (4.17) by computing the DFT of an n-element vector a where n is a power of 2. Using the power of 2 for n reduces the number of roots of unity and hence saves computation time and memory space [58].

The FFT algorithm is used in the DRP simulation to convert the phase fluctuation in the time domain to the phase spectrum in the frequency domain. Signals are represented by vectors, thus the phase fluctuation is viewed as a sinusoidal waveform that is sampled at a certain rate (discrete-time signal). For a continuous-time sinusoidal signal $\cos(\omega t)$, the signal is periodic regardless of the value of ω. Such is not the case for a discrete-time sinusoid. A discrete-time signal $\cos(\Omega t)$ is periodic only if $\frac{\Omega}{2\pi}$ is a rational number [60].

The Matlab function for the FFT algorithm is given as [59]:

$$\mathrm{Y} = \mathrm{fft}(\mathrm{X}, \mathrm{n}) \tag{4.18}$$

where the *fft* function returns the n-point DFT of the vector X. If the length of X is less than n, then X is padded with trailing zeroes to length n. If the length of X is greater than n, the vector X is truncated. In the DRP simulation, the time vector X in (4.18) defines the phase fluctuation in the time domain. The sampling frequency F_s is the inverse of the time step (distance between two adjacent time points) for the time vector X. According to the sampling theorem in [62], the sampling frequency F_s should be at least twice the signal bandwidth for signal reconstruction from the samples for band-limited signals. Band-limited signals have a finite length in the frequency domain. Time-limited signals have a finite length in the time domain. A signal cannot be time-limited or band-limited simultaneously [60]. Since finite vectors are used in the FFT computation, the time vector is time-limited. For discrete-time and time-limited signals, we have a periodic waveform in the spectrum with a period corresponding to the sampling frequency F_s. Due to time-limited signals, the spectrum consist of periodically overlapping cycles. Due to this overlap, it is no longer possible to reconstruct the original signal. The signal overlaps are known as aliasing [60]. The region of interest in the spectrum is between zero and the Nyquist frequency (i.e. half the sampling frequency) for a total of *n/2* points [59]. The time vector is a discrete-time and time-limited signal formed by choosing an initial time of one cycle, the final time of that same cycle, the time step, and the total number of cycles or periods. It is impossible to eliminate aliasing for time-limited signals but we can reduce the aliasing error by increasing the sampling frequency F_s [60].

The frequency resolution is defined as the distance between each frequency point in the spectrum. The frequency resolution is given by the following equation [60]:

$$F_o = \frac{F_s}{n} \tag{4.19}$$

where F_s is the sampling frequency and n is the number of frequency points in the FFT (4.18). When n is large, we have smaller distance between each frequency point in the spectrum and hence the graph can display more points (*n/2*). The sampling frequency F_s is found by dividing the time period of one cycle in *X* with the number of discrete time points within that cycle (sampling rate) and performing the inverse. From (4.19), when the sampling frequency F_s for *X* is low we also have lower frequency steps since the *n/2* points in the spectrum cover a smaller frequency range (DC to half the sampling frequency). The oscillation frequency is the inverse of the time period of one cycle in *X*. The sampling frequency and bandwidth of the signal (oscillation frequency) are proportional and related by the sampling rate factor:

$$F_s = r \cdot B \tag{4.20}$$

where *B* is the bandwidth of the signal and the sampling rate factor $r \geq 2$.

To summarize, having a large *n* and a smaller sampling and oscillation frequencies will result in smaller frequency steps and hence greater frequency resolution according to (4.19). However, there is an increase in the aliasing error for time-limited signals when we decrease the sampling frequency $F_{s.}$ When the sampling and oscillation frequencies are higher, we reduce the aliasing error but we have lower frequency resolution (large frequency steps) and *n* needs to be increased further to get the same frequency step as before. Due to computational resources, it is sometimes infeasible to get an adequately small frequency step when the oscillation frequency is high. Appendix A shows the matlab program for the DRP simulation in Chapter 5.3. The signal bandwidth is 811.4 Mhz after noise injections. The sampling frequency is approximately eight times the bandwidth to reduce the aliasing error. To achieve a frequency resolution between 5 to 10 kHz we set the number of frequency points *n* to be 2^{20} according to equation (4.19).

Chapter 5

SIMULATION AND MEASURED RESULTS

5.1 INTRODUCTION

In this chapter phase fluctuation (time domain) and phase noise (frequency domain) simulations are performed using the DRP approach introduced in Chapter 4.4 for the different oscillator topologies introduced in Chapter 2. Phase fluctuation simulation results are given in Chapter 5.2. Comparisons are made between the LTV and NLTV models to show how the memory property and the phase fluctuation definition plays a role in realistic phase noise prediction. In Chapter 5.3, phase noise simulation results using the NLTV model are given for a modified 810-MHz CMOS cross-coupled LC oscillator design. The simulation results are compared against the measurement results. Phase noise simulations for a BJT Colpitts oscillator using the NLTV model are given in Chapter 5.4 to show the phase noise characteristics due to $1/f$ and thermal noise. In Chapter 5.5 a cross-coupled 1-MHz CMOS oscillator design example is used to compare the phase fluctuation results for different flicker noise models introduced in Chapter 3 for the NLTV model.

The DRP simulation was implemented using Matlab v. 6.5. The 2003 Cadence Virtuoso Schematic Editor, Layout Editor, and Spectre simulator with BSIM3v3 models were used to design and simulate the 810-MHz CMOS cross-coupled LC oscillator design. The Matlab programs (.m files) used in the DRP simulations are shown in Appendix A, Appendix B, and Appendix C.

5.2 PHASE FLUCTUATION SIMULATION: LTV MODEL VS NLTV MODEL

Cadence Spectre simulation is used to find the ISF function for a particular oscillator design. But we first consider an ideal VCO with a perfectly sinusoidal ISF waveform. We want to make a phase fluctuation comparison between both models to illustrate how the recursive-memory algorithm (4.13) differs from the LTV equation (4.10) in dealing with phase changes due to impulse injections. Thus only step 5 of the DRP is performed using an ideal ISF waveform. In real life applications, the ISF function is not perfectly sinusoidal due to the parasitics of the circuit components and transistor devices in the oscillator. But in order to illustrate the fundamental differences between the LTV and NLTV models we simulate using an ideal ISF waveform. In the first case, we have a symmetrical sinusoidal ISF waveform as shown in fig. 5.1. The second case involves an asymmetrical sinusoidal ISF waveform illustrated in fig. 5.2. Phase change comparisons will be made between the LTV model and the NLTV model for both cases.

The LTV model (4.10) accounts for the past by adding all the phase shifts due to earlier noise injections. The phase fluctuation leading to phase noise is the total integrated phase shifts up into the present time and is always in reference to the original noiseless waveform. The NLTV model (4.13) accounts for previous noise injections by the constant phase shifting of the oscillator waveform (or ISF). In this model the phase fluctuation at a particular time represents the actual phase change the oscillator experiences at that time (the current phase shift) as opposed to the total integrated phase shifts. Thus the phase noise is viewed as the continuing phase disturbance of the oscillator and is due to the real-time changes in the phase. The phase fluctuation is referenced to the current phase of the oscillator waveform since the original phase information before the noise injections has long been forgotten [53].

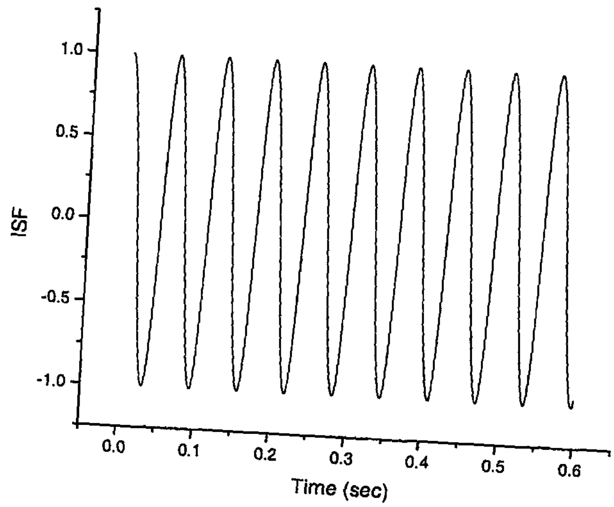

Fig. 5.1: Ideal symmetrical sinusoidal ISF waveform.

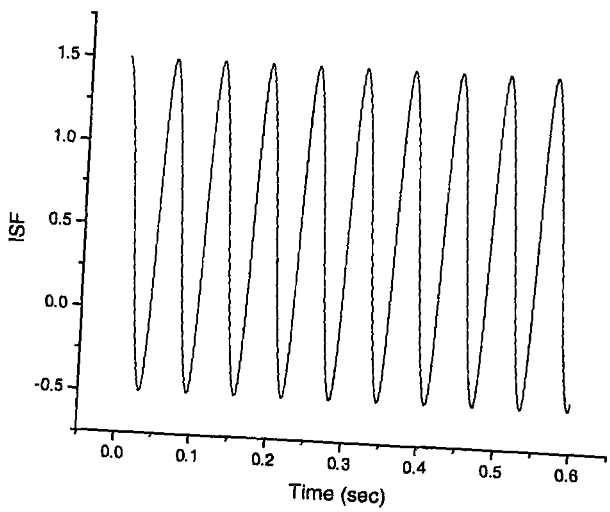

Fig. 5.2: Ideal asymmetrical sinusoidal ISF waveform.

1) Single impulse injection at the least sensitive point on ISF

According to the LTV phase noise theory, injecting an impulse when the oscillator is least sensitive to phase perturbation (i.e. the zero crossing point on the ISF) results in zero or minimal phase change. Fig. 5.3 gives the simulation result for this injection scenario. The phase was computed using the NLTV model (4.13) and LTV model (4.10), both yielding the same result. This is true for either a symmetrical or asymmetrical ISF waveform. In accordance to the LTV theory for phase noise, we have zero phase-shift after the impulse injection.

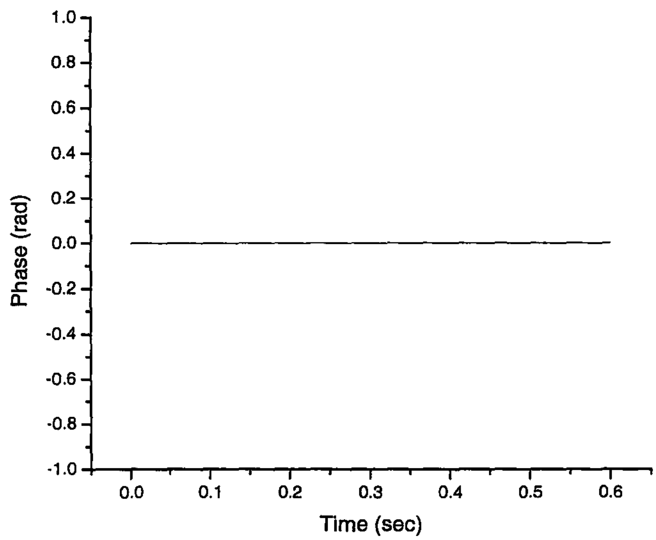

Fig. 5.3: Phase fluctuation for single impulse injection at least sensitive point.

2) Single impulse injection at a more sensitive point on ISF

When the impulse is injected when the oscillator is more sensitive to phase perturbation (i.e. near the peaks of the ISF), we expect greater phase change according to the LTV theory. This result is shown in fig. 5.4. Phase computation using the NLTV and

LTV models yields the same results for this scenario. With figs. 5.3 and 5.4, we have shown that the NLTV model takes into account time variance and makes the same predictions as the LTV model for a single impulse injection. Both the symmetrical and asymmetrical ISF cases yield similar results.

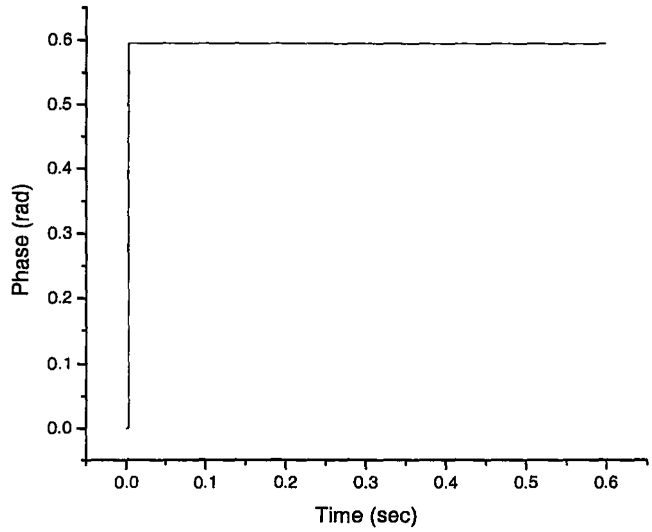

Fig. 5.4: Phase fluctuation for single impulse injection at more sensitive point.

3) Periodic impulse injection using the symmetrical ISF waveform

Impulses are injected periodically into the oscillator system instead of a single point injection in the previous two cases. Using the NLTV model, the phase computation result is shown in fig. 5.5 for the symmetrical ISF case.

Due to the periodic injections, the oscillator now experiences phase diffusion. Phase diffusion is the process in which the phase of the oscillator gradually spans a range of values (phase swing) as seen in fig. 5.5. Due to the memory property incorporated into the NLTV model, the phase traces the ISF waveform in a discrete manner for periodic impulse injections. The real-time phase fluctuation is symmetrical about the zero phase axes due to the symmetry of the ISF curve.

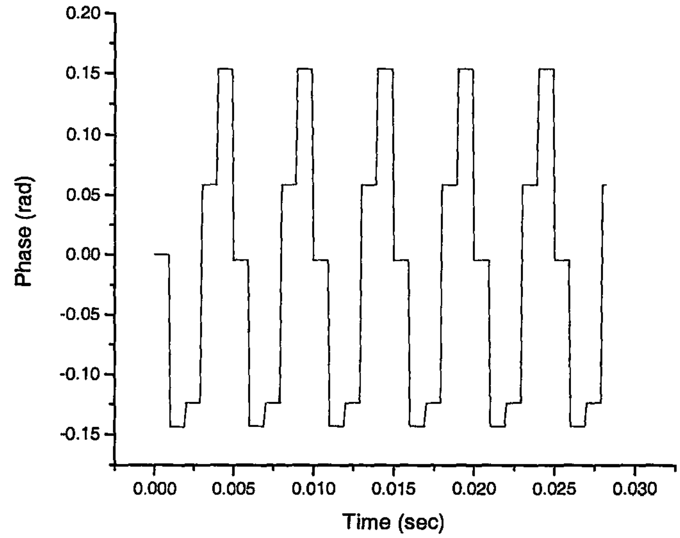

Fig. 5.5: NLTV real-time phase fluctuation for periodic impulse injection.

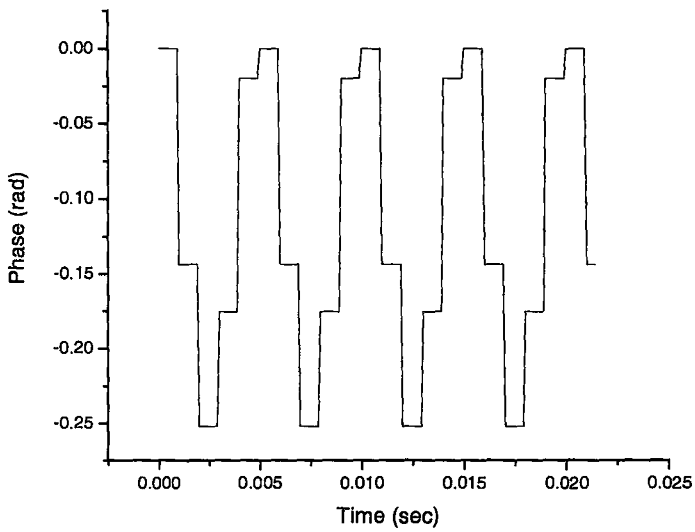

Fig. 5.6: LTV integrated phase fluctuation for periodic impulse injection.

The results of the LTV model are shown in fig. 5.6. Due to the integration nature of the algorithm, the phase fluctuation (interpreted as the total integrated phase shift in this model) does not trace the ISF curve and is non-symmetrical about the zero phase axes. In both models the phase swing is reasonably small leading to adequate phase noise performance.

4) Periodic impulse injection using the asymmetrical ISF waveform

Impulses are injected periodically into the oscillator system using the asymmetrical ISF waveform in fig. 5.2. The NLTV model results for the real-time phase fluctuation is shown in fig. 5.7. Due to the memory property, the phase traces the ISF waveform and is positively asymmetrical. The phase swing is also within reasonable limits. Using the LTV model, the integrated phase fluctuation is shown in fig. 5.8. In this model, each impulse injection has a corresponding phase shift linked by the time of injection. The LTV model simply sums up the phase shifts for each impulse injection. For example if the first impulse is injected at time x and the second impulse is injected at time y, then the corresponding phase shifts is derived from the ISF waveform at time x and time y. The LTV algorithm adds up the two phase-shifts at x and y to compute the overall integrated phase. Thus if we do not bound the phase by 180 degrees, the phase will increase with time due to the integration of the periodic phase shifts and the positively asymmetrical ISF. Since the ISF has a positive average, the result of integration over a large period of time results in the increasing trend of the phase. If the 180 and –180 degree bounds were placed on the unbounded LTV model phase curve, the phase swing would be unrealistically large. As mentioned above, the reason for the great phase perturbation is due to the asymmetrical ISF and the integration nature of the LTV algorithm. The exceedingly large phase swing will result in unrealistic poor phase noise prediction for the LTV model.

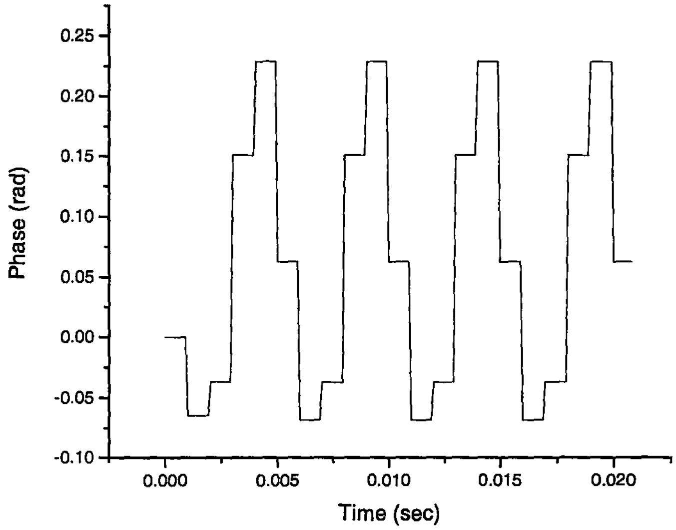

Fig. 5.7: NLTV real-time phase fluctuation for periodic impulse injection.

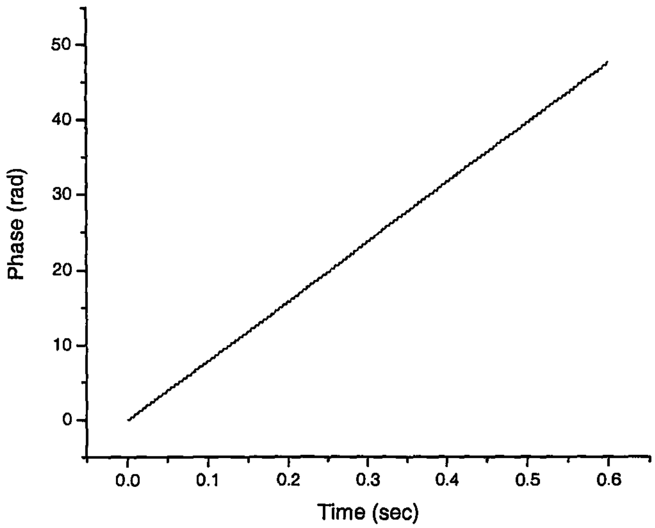

Fig. 5.8: LTV integrated phase fluctuation for periodic impulse injection.

5) Low-frequency thermal noise injection using symmetrical ISF

In the thermal noise injection simulation sinusoidal waveforms with constant amplitudes and frequencies ranging from 200 kHz to 100 MHz (frequency step of 500 kHz) are integrated in the time domain and injected together into the system. Fig. 5.9 shows the simulation results using the NLTV model with a symmetrical ISF. The phase variation peaks ranges from 0.017 radians to –0.015 radians and is partly symmetrical due to the ISF.

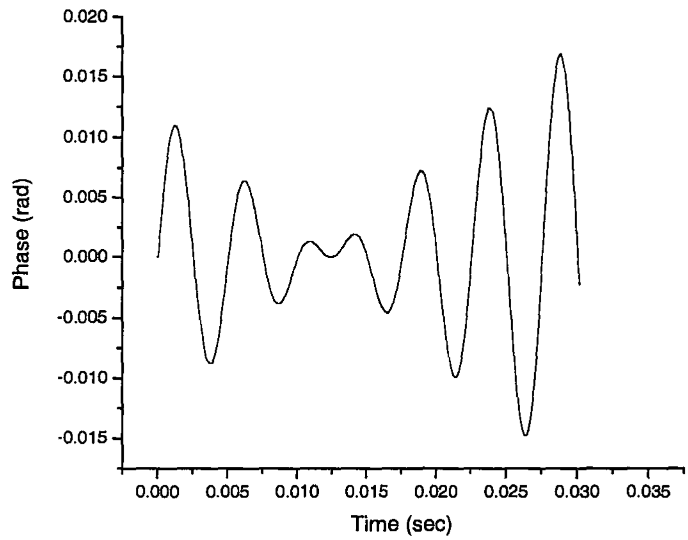

Fig. 5.9: NLTV real-time phase fluctuation for thermal noise injection (symmetrical ISF).

The thermal noise injection results for the LTV model and symmetrical ISF is shown in fig. 5.10. The phase swing is slightly larger and is asymmetrical with a positive phase average (0.27 radians to –0.1 radians). The phase spectrum has low frequency and oscillation frequency components. Due to the symmetry of the ISF, the phase variations due to thermal noise injection for both models are closely matched. Thus the phase noise performance should be similar due to the closely matched phase swings.

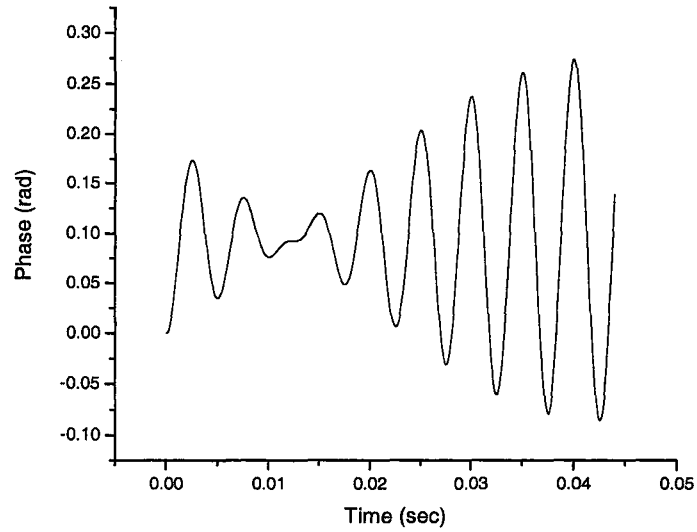

Fig. 5.10: LTV integrated phase fluctuation for thermal noise injection (symmetrical ISF).

6) Low-frequency thermal noise injection using asymmetrical ISF

The phase computation result with the 180 and –180 degree bounds for the LTV model is shown in fig. 5.11. The positively asymmetrical ISF and the integration nature of the LTV algorithm produce an increasingly unbounded phase waveform. When bounded by the 180 and -180 degree limits, we get a phase waveform that spans the entire four quadrants (-180 to 180 degrees). This unrealistically large phase variation produces extremely poor phase noise performance. The phase computation for the NLTV model is shown in fig. 5.12. Since in the NLTV model the phase fluctuation that causes phase noise is due to the real-time changes in phase instead of the total integrated phase, the phase variation is well within reasonable bounds (peaks ranging from -0.014 radians to 0.035 radians).

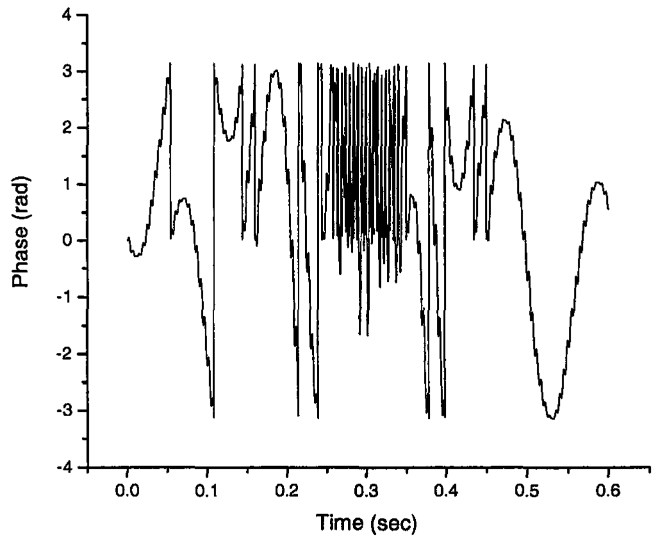

Fig. 5.11: LTV bounded integrated phase fluctuation for thermal noise injection (Asymmetrical ISF).

With the great phase swing in the LTV model due to the positively asymmetrical ISF we expect unrealistic poor phase noise performance compared to the NLTV model. When the ISF is positively asymmetrical, the LTV model inaccurately predicts great phase noise (up to –30 to –50 dBc/Hz at all frequency offsets) due to the use of integrated phase shifts to account for prior injections. The NLTV model views the phase fluctuation leading to phase noise as the real-time changes in the phase as opposed to the total integrated phase change. Thus the primary weakness of the LTV model are oscillator topologies with asymmetrical ISF waveforms.

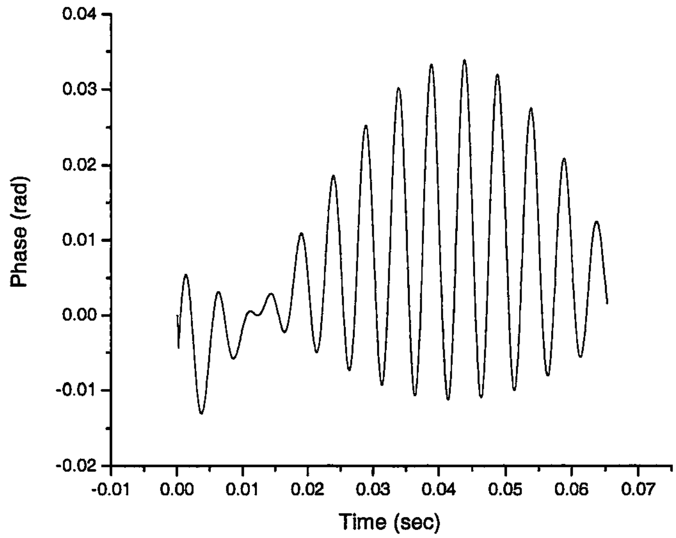

Fig. 5.12: NLTV real-time phase fluctuation for thermal noise injection (Asymmetrical ISF).

5.3 PHASE NOISE SIMULATION FOR MODIFIED CMOS CROSS-COUPLED OSCILLATOR DESIGN: NLTV MODEL VS MEASUREMENT

Consider the cross-coupled CMOS voltage controlled oscillator (VCO) in fig. 5.13 running at 810 MHz. This circuit design will be used as an example for phase noise calculation using the DRP system outlined in the previous section. It is a modification of the CMOS topology discussed in Chapter 2.2 with capacitors between the gates of the NMOS transistors and the drain. The symmetry of the half-circuits helps to improve the phase noise performance. This circuit was fabricated and measurement results were taken to compare against the corresponding phase noise simulation results. Appendix D shows the circuit schematic and specs of this oscillator design.

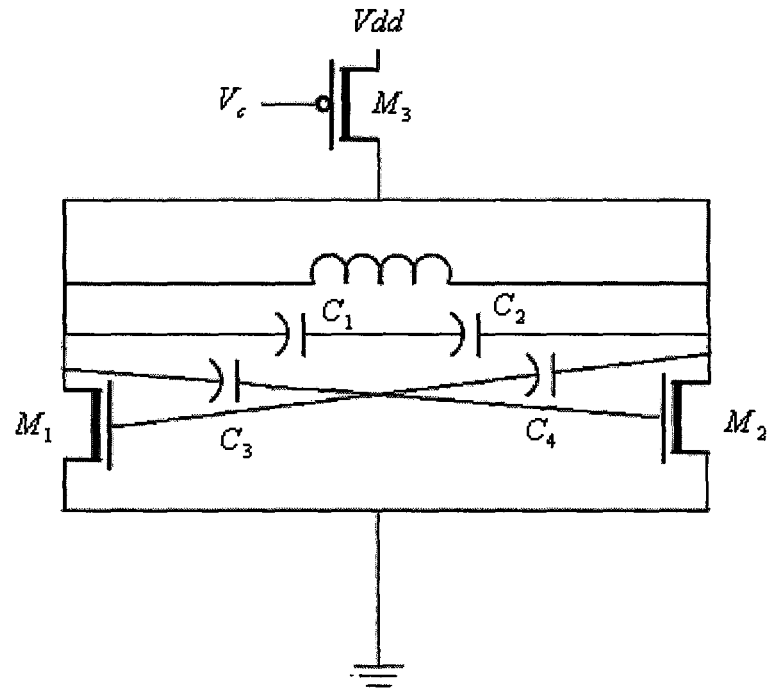

Fig. 5.13: CMOS cross-coupled VCO.

The six steps for the DRP outlined in Chapter 5 are performed for the 810-MHz oscillator design. CAD simulation using Virtuoso Spectre is performed to find the ISF function for this particular oscillator design. The ISF characterizes the sensitivity to phase noise due to noise injection for the oscillator. Impulses are injected at eight time points within an oscillation cycle and the resulting phase shifts are recorded to determine the ISF data points. The data points are extended periodically and processed by the Matlab CF tool. With these points, we use the sixth degree Fourier series fitting equation to approximate the waveform where a_0 to a_6 and b_1 to b_6 are coefficients that fit the ISF data points:

$$ISF = a_0 + a_1\cos(x\omega_o) + b_1\sin(x\omega_o) + \ldots + a_6\cos(6x\omega_o) + b_6\sin(6x\omega_o). \quad (5.1)$$

The ISF fitted curve is shown in fig. 5.14. The process also computes the RMSE to be 0.009, an acceptable approximation for the fit as discussed in Chapter 4.4. This closed formed mathematical representation of the ISF waveform is used for the implementation of the NLTV algorithm (4.13). Note that the ISF is positively asymmetrical so the simulations will be performed using the NLTV model.

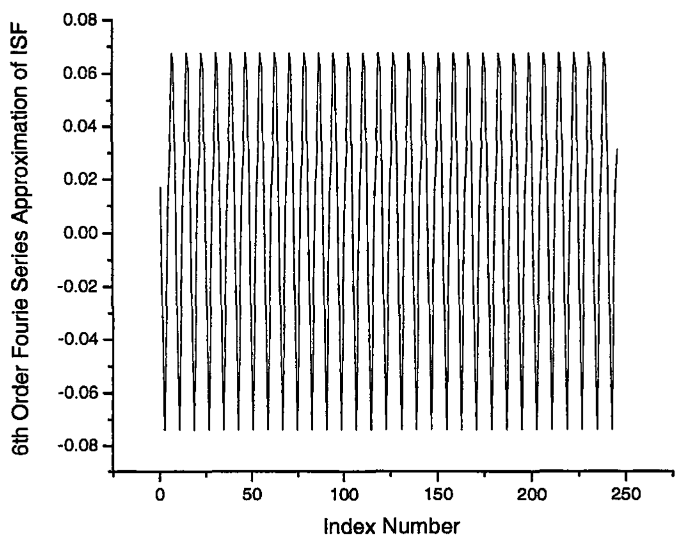

Fig. 5.14: Sixth order fourier series approximation of the ISF waveform.

Since the source of noise originates from the transistors and the transistor current changes periodically, the noise should also change with the current. Noise is minimal when the device is off and maximum during a current peak. The cyclostationary waveform shown in fig. 5.15 incorporates this periodic changing nature of noise. This waveform serves as a weighting factor for the ISF waveform discussed previously (refer to Chapter 4.4).

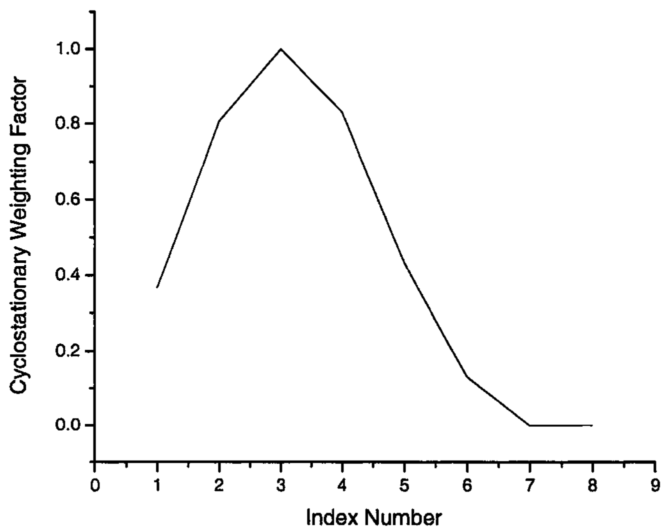

Fig. 5.15: Cyclostationary waveform.

To calculate the thermal noise injection using equation (3.4) and ignoring the body effect of the transistor, CAD simulation is used to find the transistor gain. The corresponding frequency offset sweep is from 10 kHz to 1.1 MHz with a frequency step size of 10 kHz. Since the step size is larger than the device flicker noise corner frequency, only thermal noise is considered. The DC, first harmonic and second harmonic frequency ranges are used. All the noise injections are integrated in the time domain and serve as the input into the system.

The resulting phase fluctuation in the time domain is shown in fig. 5.16. It is well within the 180 and -180 degree regions as discussed in the previous section so the phase noise prediction should be reasonable.

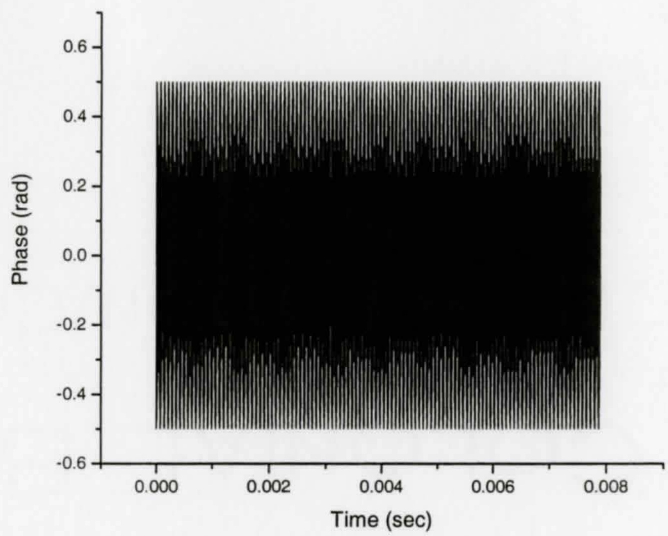

Fig. 5.16: Phase fluctuation- CMOS oscillator design.

Using the FFT with the number of frequency points N set to 2^{20}, the voltage spectrum in the frequency domain can be found. Due to the high number of frequency points, the simulation consumes many computer resources and requires a substantial amount of time to complete. All the side-band noise is surrounding the carrier or oscillation frequency As we move away from the carrier frequency the side-band noise diminishes. If we convert voltage to phase noise, we get the phase noise plot shown in fig. 5.17.

We are only interested in the peaks generated by the FFT simulation. Note that the simulation generates local maximum peaks at various frequencies even though the general trend is phase noise reduction as we move away from the carrier frequency. The frequency-offset sweep is from 0 to 1.1 MHz for the DC, first harmonic and second harmonic frequency regions. The noise injections at these frequencies are translated to frequency offsets from the carrier frequency shown as peaks in the phase noise graph. All the peaks are measured relative to the center frequency thus we have 0 dBc/Hz at the carrier. Some of the phase noise points include:

- -91 dBc/Hz @ 100 kHz offset
- -86 dBc/Hz @ 80 kHz offset
- -77 dBc/Hz @ 40 kHz offset

The difference between the 120 kHz and 1.02 MHz offset points is –23 dBc/Hz for one decade. Fig. 5.18 shows a comparison between the DRP simulation using the NLTV model (fig. 5.17), Cadence Spectra simulation and measurement data for a frequency range from 25 kHz to 100 kHz. The average difference between the DRP simulation and measurement is within 4.95 dBc/Hz. The DRP simulation predicts approximately –89 dBc/Hz at the 90 kHz offset while the measurement result reads –93 dBc/Hz at the same offset. At this offset, the simulation and the measurement readings are closely matched with a difference of approximately 4 dBc/Hz. The differences arise due to the accuracy of the noise models and the use of deterministic time-domain signals for the input noise. The

Cadence Spectra simulation and measurement readings have a difference of about 9 dBc/Hz at this offset.

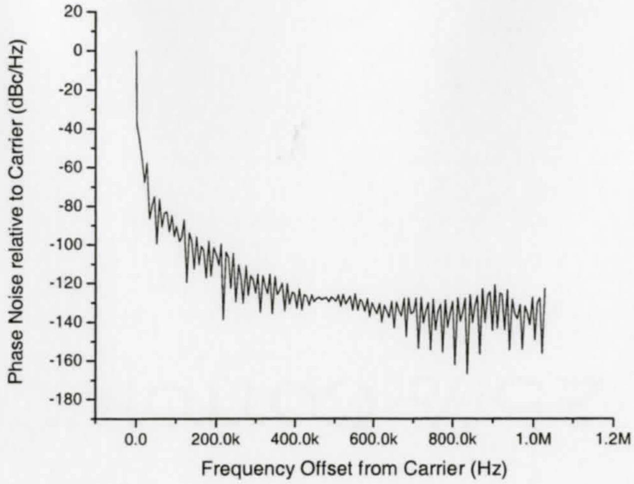

Fig. 5.17· Phase noise simulation – NLTV model.

TABLE 5.1. Phase Noise Comparisons

Data Source	Phase Noise (dBc/Hz @ 90 kHz offset)
DRP Simulation using NLTV model	- 89
CAD Simulation (Cadence Spectra)	- 101.8
Measurement	- 93

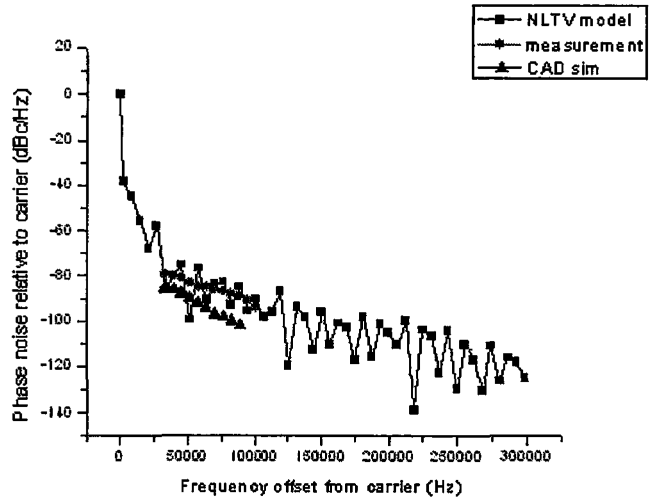

Fig. 5.18: Phase noise comparison - NLTV model vs. CAD simulation and measurement.

5.4 PHASE NOISE SIMULATION FOR BJT COLPITTS OSCILLATOR DESIGN

The NLTV Model is used for the phase noise computation of a 62-MHz BJT Colpitts oscillator shown in fig. 5.19. From the simulation in [5], we can get the ISF curve and current/voltage characteristics. As mentioned in Chapter 2.3, the collector current in the Colpitts oscillator only flows during a short interval coinciding with the peaks of the tank voltage resulting in better phase noise performance.

Fig. 5.20 gives the simulated voltage and current characteristics for this oscillator design used for the phase noise calculation and the cyclostationary effect. The design parameters for the oscillator are the following [5]:

- $C_1 = 200$ pF

- $C_2 = 40$ pF
- $I = 500\ \mu$A
- $R = 10$ kΩ
- $L = 200$ nH
- $V_{swing} = 14$ V
- $ISF_{amp} = 1$

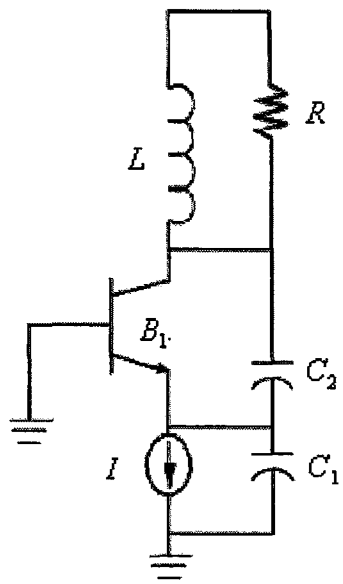

Fig. 5.19: BJT Colpitts oscillator.

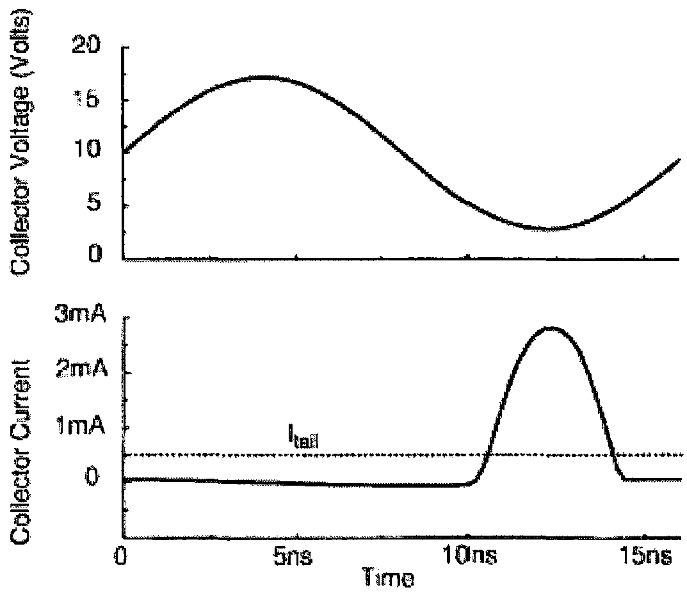

Fig. 5.20: CAD simulated voltage and current characteristics [5].

The CET NE68519 BJT is used for the devices in this simulation scenario. The experimental flicker and thermal noise characteristics are shown in reference [55] for V_{CE} = 3 V and I_C = 5mA. It is assumed that the noise parameters apply to the BJT Colpitts oscillator design during a cycle. This assumption is made since the purpose of this section is to analyze the general phase noise trends due to flicker and thermal noise and the accuracy of the phase noise prediction is not the focus. The device flicker noise parameters are:

- KF = 80f
- AF = 1.35
- BF = 109

For BJT devices, the flicker noise model is given by the equation

$$I_f = KF\left(\frac{IB^{AF}}{f}\right). \tag{5.2}$$

Thus, we have $I_f = 1.1 \cdot 10^{-19} / f$ for the flicker noise and a corner frequency of 9.5 kHz [55]. The corner frequency describes the meeting point between the flicker and thermal noise.

The frequency-offset sweep is from 2 kHz to 1 MHz with a step size of 2 kHz. Since the step size is now sufficiently small enough (due to the lower oscillation frequency of 62 MHz), flicker noise can be considered. During the region between 2 kHz and 9.5 kHz, flicker noise is injected into the system. After the 9.5 kHz point, we have thermal noise injection. In this first case, the cyclostationary effect is ignored to see its effect on phase noise. Using the NLTV model for phase noise simulation with the number of frequency points N set to 2^{20} and turning off the cyclostationary effect, the resulting phase noise result is shown in fig. 5.21. The phase noise points include:

- -104 dBc/Hz @ 10 kHz offset
- -120 dBc/Hz @ 100 kHz offset
- -141 dBc/Hz @ 1 MHz offset

Theoretically, the $1/f$ and thermal regions yields a slope of –30 dBc/decade and –20 dBc/decade respectively. In our simulation, the $1/f$ region yields a slope of approximately – 26 dBc/decade. In the thermal noise region from 100 kHz to 1 MHz we have an approximated slope of –21 dBc/decade. The differences arise due to the accuracy of the noise models and the use of deterministic time-domain signals for the input noise.

With the cyclostationary effect turned on, the advantages of the Colpitts oscillator topology are utilized. The corresponding phase noise is shown in fig. 5.22. As can be seen, the phase noise is lower than before (-128 dBc/Hz compared to –120 dBc/Hz at 100 kHz offset) due to the topology.

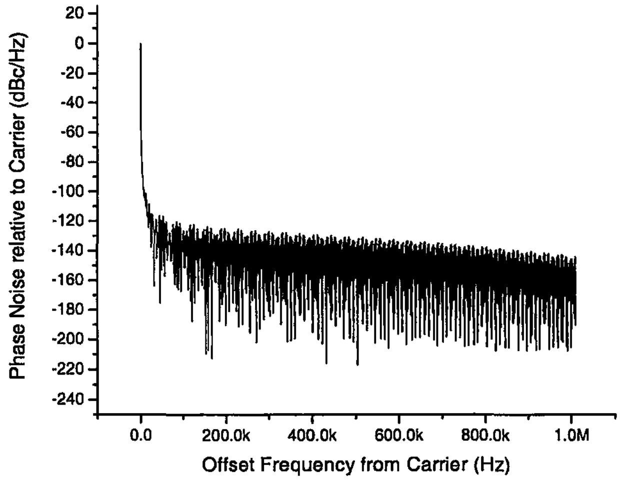

Fig. 5.21: Phase noise simulation for BJT Colpitts with cyclostationary effect turned off.

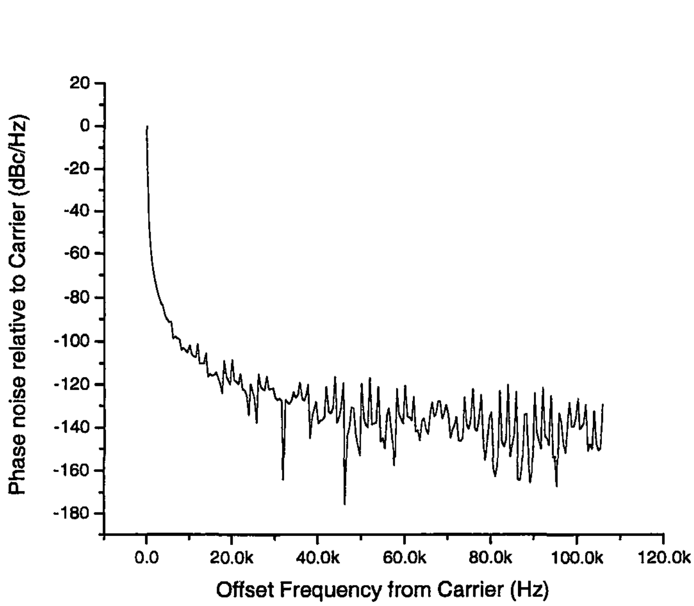

Fig. 5.22: Phase noise simulation for BJT Colpitts with cyclostationary effect turned on.

5.5 PHASE FLUCTUATION SIMULATION FOR CMOS CROSS-COUPLED OSCILLATOR DESIGN: FLICKER NOISE MODEL COMPARISONS

This section uses the *1/f* models discussed in Chapter 3.3 to calculate the phase noise of a CMOS cross-coupled design example. This section compares the effect of different flicker noise models on the phase noise calculated using the NLTV model. Note that the design is an example and it was never implemented. The only purpose of the design example is to relate the device noise physics with the phase noise calculation algorithms. From Chapter 2, MOS transistors can be used as the energy restorer since it is an active element in the *LC* oscillator. We consider the energy restorer to be a cross-coupled CMOS system introduced in Chapter 2.2 and shown in fig. 2.3. The CMOS component restores energy and provides negative differential resistance that cancels the physical resistance of the network.

For the CMOS oscillator phase noise calculation, only the noise from the n-channel MOS transistor will be taken into account. The following are the design specs:

- a gate DC bias of 1.9 volts in the saturation region under strong inversion conditions
- small-signal voltage AC swing from +0.35 to –0.35 volts
- operating frequency of 1 MHz

Thus the transistors are always assumed to be in saturation and strong inversion so the MF Model and the Non-Uniform Trap CDF models for flicker noise are valid (refer to Table 3.1 in Chapter 3).

Micropower CMOS oscillators consume very low power (in the micro-Watt range) by using the weak-inversion region of MOS transistors [56]. These oscillators will need to use the General Inversion CDF 1/*f* noise model applied to weak inversion proposed in [50].

For our simulation purposes, we use H. Fabricator from [51] to get the following n-channel MOS transistor parameters for flicker noise:

- gate oxide = 775 Å
- channel area is 80x6 $(\mu m)^2$
- flicker η slope is 0.70
- $N_T kT$ is $1.0x10^{15}$

Other device parameters for 1/*f* noise include:

- $C_{ox} = 4.46x10^{-4} \quad pF/(\mu m)^2$
- Hooge parameter $\alpha \approx 2x10^{-3}$
- effective mobility ratio $\frac{\mu_f}{\mu_{eff}} \approx 1$
- $C_{gs} \approx \frac{2}{3} WLC_{ox}$ (transistor in saturation)
- MOS threshold voltage for strong inversion $V_T = 0.7$ V

Using the above parameters and the flicker noise equations given in Table 1, the flicker noise can be calculated for each of the two models:

Mobility fluctuation model:

$$\frac{i^2_{MF-1/f}}{\Delta f} = g_m^2 \frac{V^2_{MF-G}}{\Delta f} = \frac{8.9x10^{-18}}{f} \frac{A^2}{Hz} \tag{5.3}$$

Non-uniform trap density CDF model:

$$\frac{i^2_{CDF-1/f}}{\Delta f} = g_m^2 \frac{V^2_{CDF-G}}{\Delta f} = \frac{4.84x10^{-17}}{f} \frac{A^2}{Hz} \tag{5.4}$$

Since the oscillator frequency is set to 1 MHz, the inductance and total tank capacitance can be found:

- $\omega_o = \frac{1}{\sqrt{LC}} = 2\pi \cdot 10^6$ rad/s

- L = 25 nH

- C = 1 μF

Using the flicker noise equations from (5.3) and (5.4) and all the circuit parameters, the phase noise can be calculated using the NLTV model.

The frequency step size is set to 2 kHz and three flicker noise parameters will be compared with one another:

1. *Flicker1* = $8.9x10^{-18}$ A^2 (from MF Model equation (5.3))

2. *Flicker2* = $4.84x10^{-17}$ A^2 (from CDF Model equation (5.4))

3. *Flicker3* = $1.0x10^{-15}$ A^2

Flicker1 and *Flicker2* parameters are from the MF and CDF flicker noise equations given in (5.3) and (5.4). Note that the *Flicker2* value is higher than the *Flicker1* value. This implies that the CDF Model predicts slightly more noise than the CF Model does for this design example. *Flicker3* is a test parameter with noise value higher than both *Flicker1* and *Flicker2*. We expect the *Flicker3* simulation to have the highest phase variance (and phase noise) while *Flicker1* has the lowest phase variance.

Fig. 5.23 shows the phase fluctuation results for the three flicker noise parameters using the NLTV model. As expected, the *Flicker1* simulation (MF Model) has the least phase fluctuation since it has the lowest flicker noise parameter. The *Flicker2* simulation

(CDF Model) has a higher phase fluctuation. Since the *Flicker3* parameter has the highest value, it shows the greatest phase fluctuation. It should be noted that the ratio between the *Flicker3* and *Flicker1* parameters is greater than the ratio between the *Flicker2* and *Flicker1* parameters but the *Flicker3* incremental change in phase is less than the incremental phase change for *Flicker2*. This is a property of non-linearity between the input noise current and the output phase fluctuation (NLTV model).

The *Flicker1* simulation (MF model) shows a lower phase noise than the *Flicker2* simulation (CDF model) with an average difference of approximately 2 dBc/Hz at 520 to 640 kHz offset from the carrier. Thus using different flicker noise models for phase noise simulation results in different results for phase variance and phase noise. In this design example, the MF and non-uniform trap density CDF models yielded different parameter values resulting in a slight difference of approximately 2 dBc/Hz in phase noise.

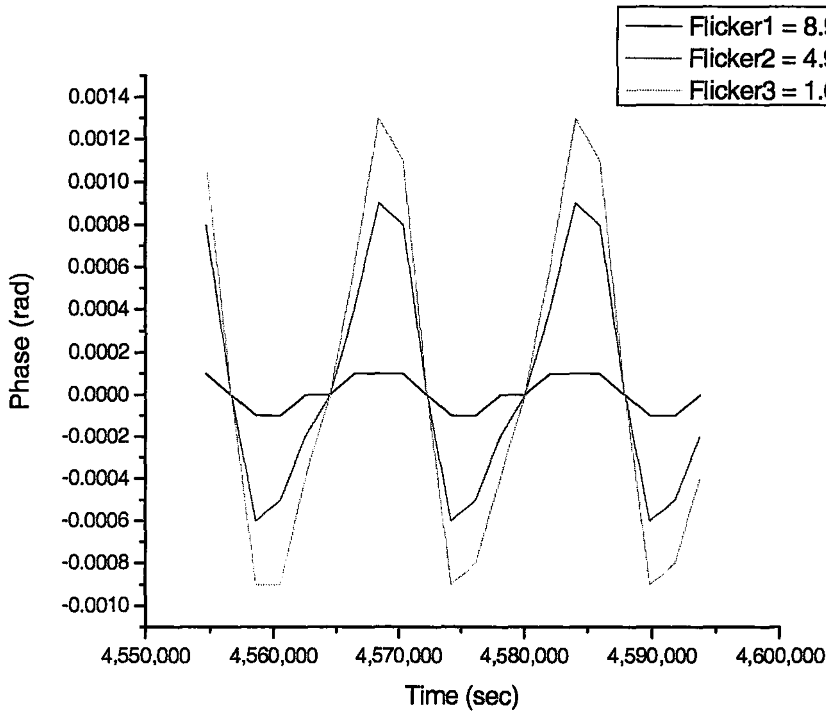

Fig. 5.23: Flicker noise simulation: phase fluctuation comparison.

Chapter 6

CONCLUSIONS

This thesis introduced the concept of memory in phase noise systems and how it has been ignored in previous phase noise research. The Non-Linear Time Varying (NLTV) model incorporates the memory property of phase. The Discrete Recursive Procedure (DRP) was introduced to implement the NLTV model and provide a systematic way for phase noise calculation.

Simulations were performed by following the steps in the DRP. With positively asymmetrical ISF waveforms, the LTV model predicted unrealistic large phase fluctuations since it uses total integrated phase shifts. The NLTV model predicted realistic phase fluctuations and phase noise performance due to the incorporation of the memory property and the use of the real-time changes in phase instead of the total integrated phase shifts. With symmetrical ISF waveforms, the difference between the two models were notably smaller and the phase fluctuations more closely matched. Thus the primary weakness of the LTV model are oscillator topologies and designs that have an asymmetrical ISF. However in most oscillator designs the ISF is never perfectly symmetrical due to the circuit components, devices and the design topology itself. As the level of symmetry decreases, phase noise predictions from the LTV model become more inaccurate. On the other hand, the NLTV model offers realistic phase noise predictions regardless of the symmetry of the ISF waveform.

The DRP phase noise prediction using the NLTV model closely matched the measurement results with an average difference within 4.5 dBc/Hz in the 810-MHz CMOS Oscillator design. At the 90 kHz offset, the simulation (-89 dBc/Hz) and the measurement readings (-93 dBc/Hz) were closely matched with a difference of approximately 4 dBc/Hz. The CAD simulation (-101.8 dBc/Hz) and measurement readings differed by approximately 9 dBc/Hz at the same offset.

For the Colpitts oscillator, the DRP simulation using the NLTV model predicted a 26 dBc/decade and –19.5 dBc/decade for the flicker noise and thermal noise regions in accordance with the theoretical –30 dBc/decade and –20 dBc/decade slopes. The Non-Uniform Trap Density CDF flicker noise model predicted more phase noise (2 dBc/Hz at 580 kHz offset) than the MF flicker noise model for the CMOS cross-coupled oscillator design example using the NLTV model. This shows that the noise source model affects the phase noise. In order to achieve an accurate phase noise prediction a more accurate noise source model is needed.

The DRP simulation uses deterministic time-domain signals to represent the input noise from the device to calculate the phase fluctuation in the time domain and the phase noise power in the frequency domain. As a future improvement for the accuracy of the DRP approach, stochastic random signals should be used for the input noise.

BIBLIOGRAPHY

[1] C. W. Sayre, *Complete Wireless Design*, McGraw Hill, 2001.

[2] D. Tse and P. Viswanath, *Fundamentals of Wireless Communication*, Cambridge University Press, 2005.

[3] S. Chin, "Crystal, Oscillator Market Improving a Bit," Electronics Supply & Manufacturing magazine, June 2003.

[4] G. Benicio, R. Linder, A Rocha, L. de Menezes and J. Costa, "RISC Microprocessor Wireless Communication System on a Single Chip," *Proceedings of the I Student Forum on Microelectronics*, vol. 1, pp. 13-16, 2001.

[5] A. Hajimiri and T.H. Lee, "A General Theory of Phase Noise in Electrical Oscillators," *IEEE Journal of Solid-State Circuits*, vol. 33, no.2, pp. 179-194, Feb. 1998.

[6] E. J. Baghdady, R. N. Lincoln, and B. D. Nelin, "Short-Term Frequency Stability: Characterization, Theory, and Measurement", *Proc. IEEE,* vol. 53, pp. 704-722, July 1965.

[7] L. S. Cutler and C. L. Searle, "Some Aspects of the Theory and Measurement of Frequency Fluctuations in Frequency Standards," *Proc. IEEE,* vol. 54, pp. 136-154, Feb. 1966.

[8] D. B. Leeson, "A Simple Model of Feedback Oscillator Noises Spectrum," *Proc. IEEE*, vol. 54, pp. 329-330, Feb. 1966.

[9] J. Rutman, "Characterization of Phase and Frequency Instabilities in Precision Frequency Sources: Fifteen Years of Progress," *Proc. IEEE*, vol. 66, pp. 1048-1174, Sept. 1978.

[10] A. A. Abidi and R. G. Meyer, "Noise in Relaxation Oscillators," *IEEE J. Solid-State Circuits*, vol. SC-18, pp. 794-802, Dec. 1983.

[11] T. C. Weigandt, B. Kim, and P.R. Gray, "Analysis of Timing Jitter in CMOS Ring Oscillators," *Proc. ISCAS*, vol. 4, pp. 27-30, June 1994.

[12] J. McNeil, "Jitter in Ring Oscillators," *Proc. ISCAS*, vol. 6, pp. 201-204, June 1994.

[13] J. Craninckx and M. Steyaert, "Low-Noise Voltage Controlled Oscillators Using Enhanced LC-Tanks," *IEEE Trans. Circuits Syst.-II*, vol. 42, pp. 794-904, Dec. 1995.

[14] B. Razavi, "A Study of Phase Noise in CMOS Oscillators," *IEEE J. Solid-State Circuits*, vol. 31, pp. 331-343, Mar. 1996.

[15] A. Sedra and C. Smith, *Microelectronic Circuits*, Oxford, 1998.

[16] T. H. Lee and A. Hajimiri, "Oscillator Phase Noise: A Tutorial," *IEEE Journal of Solid-State Circuits*, vol 35, no. 3, Mar. 2000.

[17] A. Tasic and W. Serdijn, "Concepts of Phase Noise Tuning of Bipolar Voltage Controlled Oscillators," *Proc. IEEE ISCAS2002,* vol V, pp. 161-164, May 2002.

[18] T. H. Lee and A. Hajimiri, "Design Issues in CMOS Differential LC Oscillators," *IEEE Journal of Solid-State Circuits*, vol. 34, no. 5, May 1999.

[19] Philips Semiconductors, "Philip Semiconductor's QUBiC4 Process Technology," http://www.semiconductors.philips.com/news/backgrounders/bg0012 (current: 20 July, 2005).

[20] Synergy Microwave Corporation, "Voltage Controlled Oscillators," Synergy VCO Tutorial, http://www.synergymwave.com/products/vco/vcopdf/VCoTutorial.pdf (current: 20 July, 2005).

[21] R. Rhea, *Oscillator Design and Computer Simulation,* Noble Publishing Corporation, 2000.

[22] C. Su, S. Thoka, K. Tiew, and R. Giger, "Design of Colpitts Oscillator Using Microstrip Line Inductor Compensated for Low Q,"*Proc. MWSCAS 2002*: The 2002 45th Midwest Symposium, vol. 1, pp. I 120-123.

[23] K. Mortenson, *Variable Capacitance Diodes*, Artech, 1974.

[24] Alpha Industries, "A Colpitts VCO for Wideband Set-Top Tuner Applications," *Application Note*, http://www.alphaind.com/pdf/pages/Discrete%5CAPN1006.pdf.

[25] K. Kouznetsov and R. Meyer, "Phase Noise in LC Oscillators," *IEEE Journal of Solid-State Circuits*, vol. 35, no. 8, Aug. 2000.

[26] J. Rabaey, *Digital Integrated Circuits*, Prentice Hall, Upper Saddle River, NJ, 1996.

[27] B. Nauta, E. A. M. Klumperink, A. P. Van Der Wel, "Reduction of 1/*f* Noise in MOSFETs by Switched Bias Techniques," invited paper, *Proceedings of the 17th Norchip Conference,* pp. 60-72, Oslo, Norway, Nov. 1999.

[28] A van der Ziel, *Noise in solid-state Devices and Circuits*, John Wiley & Sons, 1986.

[29] Y. P. Tsividis, *Operation and Modeling of the MOS Transistor*, McGraw Hill, 1999.

[30] J. Goo, S. Donati, C. Choi, Z. Yu, T. H. Lee and R. W. Dutton, "Impact of Substrate Resistance on Drain Current Noise in MOSFETs," *Proceedings of Sispad 2001 182*, 2001.

[31] P. H. Handel, "Quantum 1/*f* Proximity Effect in Nanotechnology," *Proc. 8th Foresight Conference on Molecular Nanotechnology*, 2000.

[32] P. H. Handel, "The Nature of Fundamental 1/*f* Noise," *XII. Internatl. Conf. on Noise in Physical Systems and 1/f Fluctuations*, St. Louis, MO, Aug. 16-20, 1993.

[33] P. H. Handel, "1/*f* Noise - an 'Infrared' Phenomenon," *Phys. Rev. Letters 34*, pp. 1492 - 1494, 1975.

[34] P. H. Handel, "Quantum Approach to 1/*f* Noise," *Phys. Rev. 22A*, p. 745, 1980.

[35] P. H. Handel and D. Wolf, "Characteristic Functional of Quantum 1/*f* Noise," *Phys. Rev. A26*, pp. 3727-30, 1982.

[36] P. H. Handel: "The Quantum 1/*f* Effect and the General Nature of 1/*f* Noise," *Archiv für Elektronik und Übertragungstechnik (AEÜ) 43*, pp. 261-270, 1989.

[37] T. S. Sherif and P.H. Handel, "Unified Treatment of Diffraction and 1/*f* Noise," *Phys. Rev. A26*, pp. 596-602, 1982.

[38] P. H. Handel, "Any Particle Represented by a Coherent State Exhibits 1/*f* Noise," *Proceedings of the VIIth International Conference on Noise in Physical Systems and 1/f Noise* edited by M. Savelli, G. Lecoy and J.P. Nougier, North - Holland, Amsterdam, p. 97, 1983.

[39] P. H. Handel, "Coherent States Quantum 1/*f* Noise and the Quantum 1/*f* Effect," *Proceedings of the VIIIth International Conference on Noise in Physical Systems and 1/f Noise* edited by A. D'Amico and P. Mazzetti, Elsevier, New York, p. 469, 1986.

[40] P. H. Handel, "Instabilities, Turbulence and Flicker-Noise in Semiconductors I, II and III," *Zeitschrift für Naturforschung 21a*, pp. 561-593, 1966.

[41] P. H. Handel, *Noise, Low Frequency*, Wiley Encyclopedia of Electrical and Electronics Engineering, vol. 14, pp. 428-449, John Wiley & Sons, Inc., John G. Webster, Editor, 1999.

[42] P. H. Handel, "Coherent and Conventional Quantum 1/*f* Effect," *Physica Status Solidi b194*, pp. 393-409, 1996.

[43] P. H. Handel, "Fundamental Quantum 1/*f* Noise in Semiconductor Devices," *IEEE Trans. on Electr. Devices 41*, pp. 2023-2033, 1994.

[44] A. van der Ziel, "Unified Presentation of 1/*f* Noise in Electronic Devices: Fundamental 1/*f* Noise Sources," *Proc. IEEE 76*, pp. 233-258, 1988.

[45] A. van der Ziel, "The Experimental Verification of Handel's Expressions for the Hooge Parameter," *Solid State Electronics*, vol. 31, pp. 1205-1209, 1988.

[46] A. van der Ziel, A.D. van Rheenen, and A.N. Birbas, "Extensions of Handel's 1/*f* Noise Equations and their Semiclassical Theory," *Phys. Rev. B40*, pp. 1806-1809, 1989.

[47] P. H. Handel, "Noise, Low Frequency," Wiley Encyclopedia of Electrical and Electronics Engineering, vol. 14, pp. 428-449, John Wiley & Sons, Inc., John G. Webster, Editor, 1999.

[48] W. Christian, *Physlets*, Physics Applets, http://webphysics.davidson.edu/applets/applets.html (current: 1 Aug 2005).

[49] H. Tian, "Analysis of 1/*f*-Noise in Switched MOSFET Circuits," *IEEE Trans. Circuits and Systems part II*, pp. 151-157, 2001.

[50] A. Arnaud and C. Galup-Montoro, "Simple, Continuous and Consistent Physics based Model for Flicker Noise in MOS Transistors," *Proc. VIII Workshop Iberchip*, April 2002.

[51] J. Chang, A. A. Abidi, and C. R. Viswanathan, "Flicker Noise in CMOS Transistors from Subthreshold to Strong Inversion at Various Temperatures," *IEEE Trans. Electron. Devices*, vol. 41, pp. 1965-1971, Nov. 1994.

[52] W. A. Gardner, *Cyclostationarity in Communications and Signal Processing*, New York: IEEE Press, 1993.

[53] D. Ham and A. Hajimiri, "Virtual damping and Einstein Relation in Oscillators," *IEEE Journal of Solid-State Circuits*, vol. 38, no. 3, pp. 407-418, Mar. 2003.

[54] H. Sloate, "Matrix representations for sorting and the fast Fourier transform", IEEE Transactions, vol. 21, Issue 1, pp. 109-116, Jan. 1974.

[55] California Eastern Laboratories, "1/*f* Noise Characteristics Influencing Phase Noise," AN 1026 Application Note, http://www.cel.com/pdf/appnotes/an1026.pdf.

[56] T. Lin, H. Sanchez, and W. Kaiser, "Wireless Integrated Network Sensors for Tactical Information Systems," *Proceedings of the 1998 Government Microcircuit Applications Conference*, 1998.

[57] Z. Y. Chuang and W. Sansen, *Low-noise wide-band amplifiers in bipolar and CMOS technologies*, Kluwer Academic Publishers, Boston, 1991.

[58] T. Cormen, Charles Leiserson, and R. Rivest, *Introduction to Algorithms*, The MIT Press, Cambridge, Massachusetts, 1990.

[59] Mathworks, "Matlab Reference" http://www.mathworks.com/access/helpdesk/help/techdoc/matlab.html, 2005.

[60] B.P. Lathi, *Linear Systems and Signals*, Berkeley-Cambridge Press, Carmichael, California, 1992.

[61] J.W. Cooley and J.W. Tukey, "An Algorithm for the Machine Calculation of Complex Fourier Series", *Mathematics of Computation*, vol. 19, pp. 294-301, April 1965.

[62] D.A. Linden, "A Discussion of Sampling Theorem", *Proc. IRE*, vol. 47, pp. 1219-1226, July, 1959.

Appendix A

DRP SIMULATION FOR CMOS LC OSCILLATOR DESIGN - MATLAB PROGRAM

```
% clear up memory space
cwd = pwd;
cd(tempdir);
pack
cd(cwd)

% system parameters
t_first = 2.80026*10^-6
t_last = 2.801494*10^-6
sample_rate = 8;
t_int = (t_last-t_first)/sample_rate;
N=2^20;
f = 1/(t_last-t_first)
resolution = (1/t_int)/N
PI = 3.14159;

% cyclostationary waveform from CAD simulation
S = [0.3673 0.8061 1 0.83 0.4327 0.1316 4*10^(-5) 8*10^(-5)]
cyclo = S;

% time vector formation
cycles = 102;
t = t_first:t_int:cycles*t_last;

maxim = size(t)-1;
maxim = maxim(2);


% circuit and device parameters
A = 0.681;  % voltage swing
C = 3*10^(-12); % capacitance
q = C*A % max charge at node in coulombs: controls noise injection
gm = 19.95*10^(-3);
k = 1.38 *10^(-23);
T = 300;
row = 0.67;

% thermal noise calculation
thermal = 4*k*T*row*gm
m = sqrt(thermal)

% input noise injection
```

```
In = 0;
corner = 0;
for k = 10*10^3:10*10^3:1.4*10^6
  Curr = m*cos(2*PI*k*t) + m*cos(2*PI*(f+k)*t) + m*cos(2*PI*(2*f+k)*t);
  In = In + Curr;
end

In_freq1 = abs(fft(In, N));
In_freq1 = In_freq1.* conj(In_freq1) / N;

   a0 =   0.006985 % (0.006985, 0.006985)
    a1 =    0.04133  %(0.04133, 0.04133)
    b1 =      0.048  %(0.048, 0.048)
    a2 =   -0.00994  %(-0.01123, -0.008653)
    b2 =  -0.008159  %(-0.009744, -0.006575)
    a3 =  -0.005626  %(-0.007115, -0.004138)
    b3 =   0.002272  %(0.0008483, 0.003696)
    a4 =   0.000294  %(-3.727e-005, 0.0006252)
    b4 = -0.0002146  %(-0.003159, 0.00273)
    a5 =  -0.001458  %(-0.002939, 2.399e-005)
    b5 =  -0.001092  %(-0.002524, 0.0003389)
    a6 =  -0.001797  %(-0.003095, -0.0004983)
    b6 =   0.001814  %(0.0002378, 0.003389)
    w =  5.092e+009  %(5.092e+009, 5.092e+009)
    x = t;

% Fourier-Series fitted ISF waveform from CAD simulation

ISF_fit = a0 + a1*cos(x*w) + b1*sin(x*w) + a2*cos(2*x*w) + b2*sin(2*x*w) + a3*cos(3*x*w) +
b3*sin(3*x*w) + a4*cos(4*x*w) + b4*sin(4*x*w) + a5*cos(5*x*w) + b5*sin(5*x*w) + a6*cos(6*x*w) +
b6*sin(6*x*w);


% Phase Variance Computation using the MEMORY algorithm
Phase_Computation_Mem = 1
i = 1;
phase(i) = 0;
phase(i+1) = phase(i);

c = 1;
for i = 2:1:(maxim)
   if In(i) == 0
      phase(i+1) = phase(i);
   else
      phase(i+1) = cyclo(c)*(1/q)*(a0 + a1*cos(x(i)*w + phase(i)) + b1*sin(x(i)*w + phase(i)) +
a2*cos(2*x(i)*w + phase(i)) + b2*sin(2*x(i)*w + phase(i)) + a3*cos(3*x(i)*w + phase(i)) +
b3*sin(3*x(i)*w + phase(i)) + a4*cos(4*x(i)*w + phase(i)) + b4*sin(4*x(i)*w + phase(i)) +
a5*cos(5*x(i)*w + phase(i)) + b5*sin(5*x(i)*w + phase(i)) + a6*cos(6*x(i)*w + phase(i)) +
b6*sin(6*x(i)*w + phase(i)))*In(i);
      c = c + 1;
      if c == 8
```

```
        c = 1;
      end
    end;
  end

Y = fft(phase,N);


% Voltage Modulation

Vmod = A*cos(w*t+phase);
Y = fft(Vmod,N);
mem = Y.* conj(Y) / N;

Vmod = A*cos(w*t+0);
Y = fft(Vmod, N);
perfect = Y.*conj(Y) / N;

freq = (1/t_int)*(0:N/2)/N;
max_mem = max(mem)
max_perfect = max(perfect)

% Measured Data
measure = -1*[75 77 79 80 83 85 86 88 89 91 94]

% Plotting and Graphing
subplot(2, 3, 1)
plot(freq,mem(1:(N/2+1)))

subplot(2, 3, 2)
plot(freq-8.1042*10^8, 10*log((mem(1:(N/2+1)))/max_perfect))

% 25 kHz to 99 kHz
for k = 1:0.9:10
  hold on
  plot(k*10*10^3, measure(k), '--rs', 'MarkerSize', 10)
end

subplot(2, 3, 5)
plot(freq, In_freq1(1:(N/2+1)))
```

Appendix B

DRP SIMULATION FOR BJT COLPITTS OSCILLATOR DESIGN (CYCLOSTATIONARY TURNED OFF)- MATLAB PROGRAM

```
%*************************************8

t_first = 2.8074*10^-5
t_last = 2.8090*10^-5
sample_rate = 8;
t_int = (t_last-t_first)/sample_rate;
f = 1/(t_last-t_first)
resolution = (1/t_int)/N
PI = 3.14159;
w = 2*PI*f;

t = t_first:t_int:t_last - t_int;

cycles = 102;

t = t_first:t_int:cycles*t_last;

maxim = size(t)-1;
maxim = maxim(2);


%**************************************

A = 14;  % voltage swing
ISFM = 1; % ISF Sensitivity
VCO = A*cos(w*t);
C = 33*10^(-12); % capacitance
q = C*A % max charge at node in coulombs: controls noise injection
N = 2^20;  % num of frequency points
freq = f*sample_rate*[0:N-1]/N;
flicker = 1.1*10^(-19); % 1/f noise parameter: controls noise injection

%************ NOISE INTEGRATION
In = 0;
corner = 10*10^3
for k = 2*10^3:2*10^3:1*10^6
if k < corner
   m = sqrt(flicker*1/k);
   Curr = m*cos(2*PI*k*t);
else
```

```
   Curr = m*cos(2*PI*k*t);
end;
   In = In + Curr;
end

%************* LOOP
In_freq = (abs(fft(In, N))).^2;


 % memory effects
i = 1;
phase(i) = 0;
phase(i+1) = phase(i);

for i = 2:1:maxim
   if In(i) == 0
      phase(i+1) = phase(i);
   else
      phase(i+1) = (1/q) * ( ISFM*cos(w*t(i)+PI/2 + phase(i)) ) * In(i);
   end;
end
Y = fft(phase,N);
Pyy = abs(Y);

Vmod = A*cos(w*t+phase);    % voltage modulation
Y = fft(Vmod,N);
Pyy2 = abs(Y);
mem = Pyy2;
max_mem = max(mem);

subplot(1, 2, 1)
plot(freq, In_freq, 'b')
title('Input Noise')
xlabel('frequency (Hz)')

subplot(1, 2, 2)
plot(freq, 10*log(0.5*mem.^2/(0.5*max_mem^2)), 'r')
title('Phase Noise Comparison Relative to Carrier(dB/Hz)')
xlabel('frequency (Hz)')
```

Appendix C

DRP SIMULATION FOR FLICKER NOISE SIMULATION USING 1-MHZ CMOS OSCILLATOR DESIGN - MATLAB PROGRAM

```
%**************************************8
N = 2^12;  % num of frequency points
t_first = 2.8*10^-5
t_last = 2.9*10^-5
sample_rate = 8;
t_int = (t_last-t_first)/sample_rate;
f = 1/(t_last-t_first)
resolution = (1/t_int)/N
PI = 3.14159;
w = 2*PI*f;

t = t_first:t_int:t_last - t_int;

cycles = 18;

t = t_first:t_int:cycles*t_last;

maxim = size(t)-1;
maxim = maxim(2);


%***************************************

A = 0.35;  % voltage swing
ISFM = 1; % ISF Sensitivity
VCO = A*cos(w*t);
C = 1*10^(-6); % capacitance
q = C*A % max charge at node in coulombs: controls noise injection
freq = f*sample_rate*[0:N-1]/N;

flicker = 8.9*10^(-18);
flicker2 = 4.87*10^(-17);
flicker3 = 1*10^(-15);

%************* NOISE INTEGRATION
In = 0;
In2 = 0;
In3 = 0;
corner = 10*10^3
for k = 2*10^3:2*10^3:1*10^6
```

```
if k < corner
   m = sqrt(flicker*1/k);
   Curr = m*cos(2*PI*k*t);

   m2 = sqrt(flicker2*1/k^0.7);
   Curr2 = m2*cos(2*PI*k*t);

   m3 = sqrt(flicker3*1/k);
   Curr3 = m3*cos(2*PI*k*t);


else
   Curr = m*cos(2*PI*k*t);
   Curr2 = m2*cos(2*PI*k*t);
   Curr3 = m3*cos(2*PI*k*t);
end;
   In = In + Curr;
   In2 = In2 + Curr2;
   In3 = In3 + Curr3;
end

%************* LOOP
%In_freq = (abs(fft(In, N))).^2;


 % memory effects
i = 1;
phase(i) = 0;
phase(i+1) = phase(i);

phase2(i) = 0;
phase2(i+1) = phase2(i);

phase3(i) = 0;
phase3(i+1) = phase3(i);

ON = 1;

for i = 2:1:maxim
    if In(i) == 0
        phase(i+1) = phase(i);
     else
        phase(i+1) = (1/q) * ( ISFM*cos(w*t(i)+PI/2 + phase(i)) ) * In(i);
     end;

    if In2(i) == 0
```

```
        phase2(i+1) = phase2(i);
     else
        phase2(i+1) = (1/q) * ( ISFM*cos(w*t(i)+PI/2 + phase2(i)) ) * In2(i);
    end;

    if In3(i) == 0
        phase3(i+1) = phase3(i);
     else
        phase3(i+1) = (1/q) * ( ISFM*cos(w*t(i)+PI/2 + phase3(i)) ) * In3(i);
    end;
end

Vmod = A*cos(w*t+0);
Y = fft(Vmod, N);
perfect = abs(Y);
max_perfect = max(perfect)

Y = fft(phase,N);
Pyy = abs(Y);
Vmod = A*cos(w*t+phase);    % voltage modulation
Y = fft(Vmod,N);
Pyy2 = abs(Y);
mem = Pyy2;

Y = fft(phase2,N);
Pyy = abs(Y);
Vmod = A*cos(w*t+phase2);    % voltage modulation
Y = fft(Vmod,N);
Pyy2 = abs(Y);
mem2 = Pyy2;

Y = fft(phase3,N);
Pyy = abs(Y);
Vmod = A*cos(w*t+phase3);    % voltage modulation
Y = fft(Vmod,N);
Pyy2 = abs(Y);
mem3 = Pyy2;


subplot(1, 2, 1)
plot(freq, 10*log(0.5*mem.^2/(0.5*max_perfect^2)), 'r')
hold on
plot(freq, 10*log(0.5*mem2.^2/(0.5*max_perfect^2)), 'g')
hold on
plot(freq, 10*log(0.5*mem3.^2/(0.5*max_perfect^2)), 'b')
```

```
title('Phase Noise Comparison Relative to Carrier(dB/Hz)')
xlabel('frequency (Hz)')
h = legend('flicker1 = 8.9e-018','flicker2 = 4.9e-017', 'flicker3 = 1.0e-015',3);

subplot(1, 2, 2)
plot(t, phase, 'r')
hold on
plot(t, phase2, 'g')
hold on
plot(t, phase3, 'b')
h = legend('flicker1 = 8.9e-018','flicker2 = 4.9e-017', 'flicker3 = 1.0e-015',3);
```

Appendix D

810-MHZ CMOS OSCILLATOR DESIGN

The CAD schematic for the 810-MHz CMOS oscillator design is shown in fig. D.1 with the specific circuit components, labels, and the output buffer. The circuit is a modified version of the traditional CMOS cross-coupled oscillator. The PMOS cross-coupled pair is gone with only the NMOS pair remaining. The voltage applied to the gates of the NMOS pairs M_1 and M_2 are used to control the oscillation. When the applied gate voltage is within a certain voltage range, oscillation will appear in the circuit. There is no oscillation outside the voltage range. For example, when the applied voltage is 0.1 V there is no oscillation since the NMOS transistors are off and the energy restorer is non-functional. The voltage applied also controls the frequency value for the voltage ranges that support oscillation. The capacitors at the gates of the NMOS pair acts as an open circuit for the applied DC gate voltage to the LC tank. The purpose of the output buffer is to match the signal output with the 50-ohm resistance load when making measurements.

From the 2003 Cadence Spectra and Matlab v. 6.5 simulations, the oscillation frequency is between 810 to 815 MHz. The frequency found from measurements is 751 MHz. The difference in frequencies is due to the parasitics in the CMOS devices, inductors, capacitors, and the measurement equipment. Fig. D.2 shows the phase noise measurements for the CMOS oscillator design. In the one-decade span between frequency offsets 1 kHz to 10 kHz, we get a noise slope of approximately –30 dB/decade in accordance with theory due to flicker noise. The decade span between offsets 10 kHz to 100 kHz is approximately –20 dB/decade due to thermal noise injection. The CAD phase noise simulation yields –101.8 dBc/Hz at a 90 kHz offset from the carrier. The DRP simulation using the NLTV model predicts approximately –89 dBc/Hz at the 90 kHz offset. The measurement result is about –93 dBc/Hz at the same offset.

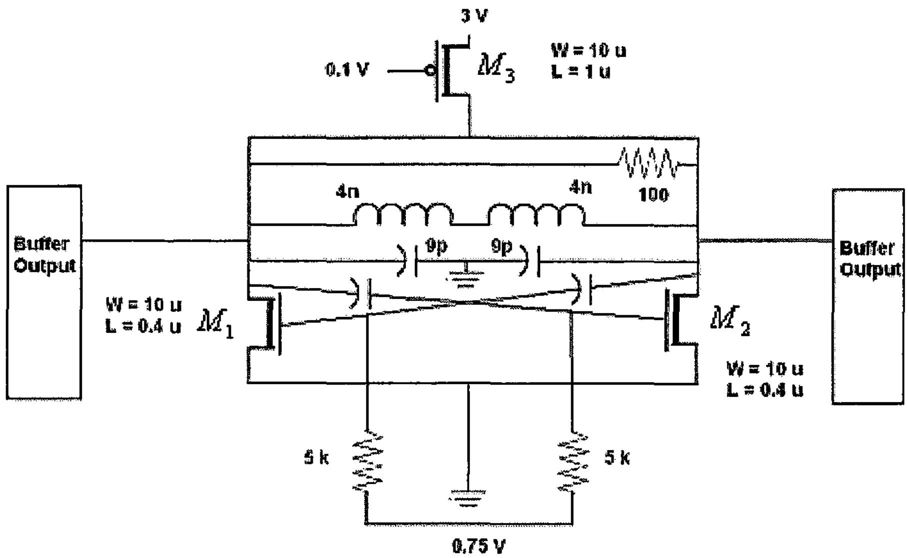

Fig. D.1: 810-MHz CMOS oscillator schematic.

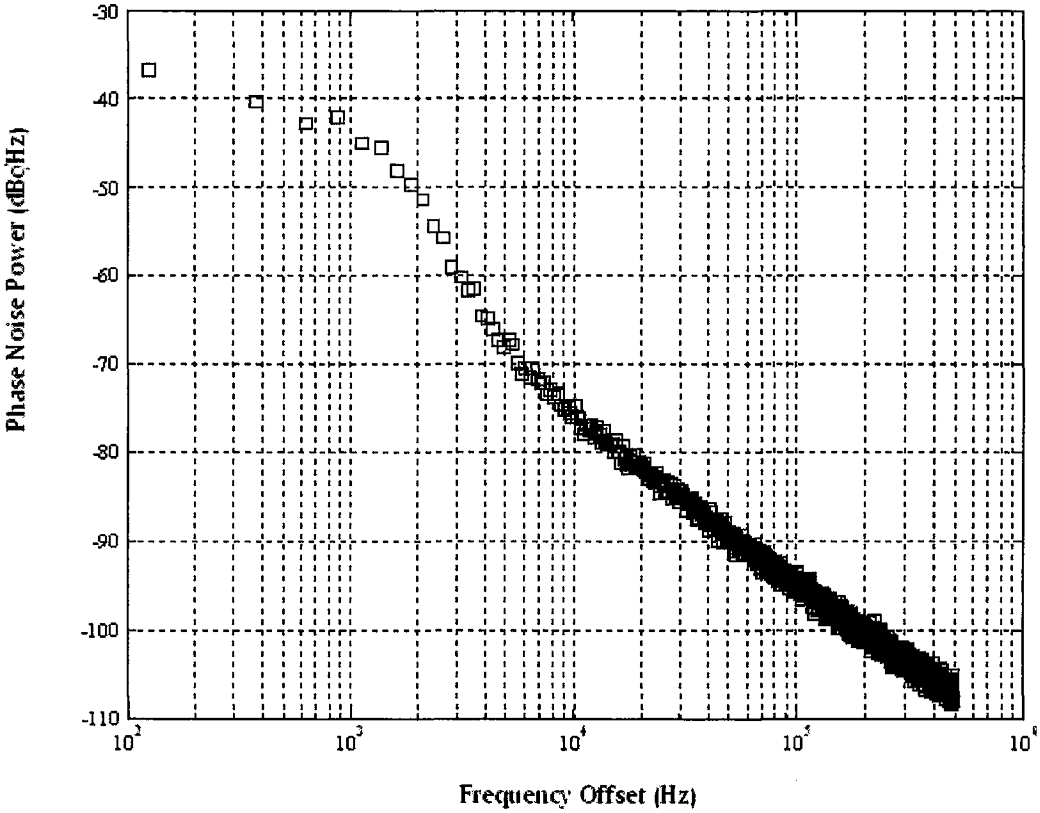

Fig. D.2: Measurement results - f=751 MHz, resolution Bandwidth = 910 Hz.